Highlights of Joint Research

Synchrotron Radiation Laboratory

The Synchrotron Radiation Laboratory (SRL) was established in 1975 as a research group dedicating to study solid state physics using synchrotron radiation. Since 1980s, SRL has been promoting the "Super-SOR" project for constructing a new synchrotron radiation facility with a third generation light source dedicated to the sciences in vacuum ultraviolet and soft X-ray (VSX) regions. In 1985, the SRL started to hold the Tsukuba branch, a branch laboratory in the Photon Factory (PF), High Energy Accelerator Research Organization (KEK). SRL maintains an undulator called Revolver, two beamlines and three experimental stations; BL-18A for angle-resolved photoemission spectroscopy and two beamlines, BL-19A and BL-19B for spin-resolved photoelectron spectroscopy and soft X-ray emission spectroscopy experiments using undulator radiation. They are fully opened to outside users for experiments using high brilliant synchrotron radiation from the undulator. The operation time of these beamlines are about 5000 hours and the number of users is more than 200 a year.

The present SRL consists of the accelerator physics group and the solid state spectroscopy group. The members of the accelerator group have been carrying out research works on the accelerator physics and developing new accelerator related technology in collaboration with other SR facilities, which play essential roles in the Super-SOR project. The spectroscopy group not only serves users at the Tsukuba branch with technical supports and advices, but also carry out their own research works on advanced solid state spectroscopy as well as instrumentation for the super SOR project.

The scientific highlights achieved in 2004 at the Tsukuba branch are found in the studies of magnetic properties of thin films. One is the study of electronic structures of Fe thin films grown on Rh(100) surface by spin-resolved photoemission (J. Phys. Soc. Jpn. 73, 2250 (2004)). It was found that the Fe films not thicker than 3 ML are magnetically dead on the Rh(100) surface due to a large strain at the Fe/ Rh(100) interface, which was supported by MCD experiments and total energy calculation of Fe films with fct structure. The other is the study of Fe(wedge)/NiO(100) system by PEEM experiments (J. Phys. Soc. Jpn. 73, 2932 (2004)). By comparing antiferromagnetic domain images of NiO(100) observed at Ni L_2 and O K edges in a Fe(wedge)/NiO(100) system, they have successfully distinguished two types of domains, namely *T*-domain originating from the crystallographic twinning effects due to the rhombohedral contraction and *S* (spin) -domain.

The accelerator group demonstrated that the emittance of the electron beam in the Super-SOR storage ring can be improved to be 3 nmrad, which will be smaller than those of the existing VUV and soft X-ray SR sources. They also made progress with the hardware design of the ring and the booster synchrotron. In the R&D of the Super-SOR project, they developed a new beam profile monitor using an X-ray imaging optics with two Fresnel zone plates and succeeded in measuring the beam size less than 6 microns and the radiation damping times with and without damping wigglers in the KEK accelerator test facility. The new orbit correction method, the eigenvector method with constraints, was experimentally studied by using the PF ring as well as the PF-AR and its excellent correction performance was demonstrated by this study.

Neutron Science Laboratory

The Neutron Science Laboratory (NSL) has been playing a central role in neutron scattering activities in Japan since 1961 by performing its own research programs as well as providing a strong general user program for the university-owned various neutron scattering spectrometers installed at the JRR-3 operated by Japan Atomic Energy Research Institute in Tokai. Under the general user program supported by NSL, 14 university-group-owned spectrometers in the JRR-3 reactor (20MW) are available for a wide scope of researches on material science, and proposals close to 300 are submitted each year, and the number of visiting users under this program reaches over 6000 person-day/year.

Triple axis spectrometers and a high resolution powder diffractometer are utilized for a conventional solid state physics and a variety of research fields on hard-condensed matter, while in the field of soft-condensed matter physics, researches are mostly carried out by using the small angle neutron scattering (SANS-U) and/or neutron spin echo (NSE) instruments. The upgraded time-of-flight (TOF) inelastic scattering spectrometer is also available from May 2005.

Major research topics on the hard-condensed matter science cover stripe order in high-Tc superconductors, and closely related 2 dimensional systems, charge and orbital ordering in CMR manganites, quadrapolar ordering in rare-earth based intermetallic compounds, spin dynamics of low

dimensional dimmer systems, etc. On the other hand, the research topics on the soft-condensed matter science cover structural characterization of polymer blends, micelles, amphiphilic polymers block copolymers, liquid crystals, proteins, inorganic gels, dynamics of brush-polymers on surface, slow dynamics of surfactants, pressure dependence of dynamics of amphiphilic membranes, and so on. In addition, there are a variety of activities on fundamental physics, neutron beam optics, developments of neutron scattering techniques.

In 2003, the Neutron Scattering Laboratory was reorganized as the Neutron Science Laboratory to further promote the neutron science with use of the instruments in JRR-3. The NSL also operates the U.S.-Japan cooperative program on neutron scattering, providing further research opportunities to material scientists who wish to utilize the neutron scattering technique for their research interests.

The details of individual studies in the JFY2004 are reported in the NSL-ISSP Activity Report vol. 12.

Supercomputer Center

The supercomputer system in the Supercomputer Center of the Institute (SCC-ISSP) is placed at the service of general researchers of condensed matter physics through the User Program conducted by the Materials Design and Characterization Laboratory (MDCL). One of its aims is to selectively promote and support huge computations.

In fiscal year 2004, which was the last one of the five-year rental period of the system, the SCC-ISSP main system consisted of two supercomputers: Hitachi SR8000/60, a distributed-memory-type parallel supercomputer with 640GB memory in total and 12x60GFlops peak performance (called System-A), and SGI Origin 2800/384, a massively parallel supercomputer with 192GB memory and 0.8x384GFlops peak performance (called System-B). Now in fiscal year 2005 they are replaced by Hitachi SR11000/48 model J1 with 2.8TB memory and 5.8TFlops peak performance, and by SGI Altix3700/1280 with 1.3TB memory and 7.7TFlops peak performance, respectively.

A project(s) can be proposed by any staff in universities or public research institutes in Japan. The projects proposed are judged by the Steering Committee of the SCC-ISSP, under which the Supercomputer Project Advisory Committee is formed to review proposals. In fiscal year 2004 totally 151 projects were approved. The total points applied and approved are listed on Table 1 below.

The research projects are roughly classified into the following three (the number of projects approved):

First-Principles Calculation of Materials Properties (55)
Strongly Correlated Quantum Systems (59)
Cooperative Phenomena in Complex, Macroscopic Systems (37)

All the three involve both methodology of computation and its applications. The results of the projects are reported in 'Activity Report 2004' of the SCC-ISSP. In the report the following four invited articles are included:

"Realization of a Computer Simulation Environment based on ITBL and Large Scale LDA and GW Calculations Performed on this Platform", by Y. Kawazoe, M. Sluiter, K. Ichinoseki, K. Ohno, S. Ishii, R. Hayashi, Y. Inoguchi, H. Adachi, H. Yamaguchi, and C. Kitagawa,
"Structural Properties of Solid Oxygen: Density Functional Study", by T. Oda,
"Quantum Number Projection and Path Integral Renormalization Group Method", by T. Mizusaki and M. Imada,
"New Type of Universality on Néel Temperatures of Quasi-Low-Dimensional Antiferromagnets", by C. Yasuda, S. Todo, K. Hukushima, F. Alet, M. Keller, M. Troyer, and H. Takayama.

The first article above is the report of a special project, by which 4 nodes of system-A were exclusively used in whole fiscal year 2004 for testing the method for the parallel usage of remote supercomputers that its authors are developing. The brief report of the fourth article is reported in this volume as a highlight of the joint-use researches.

Table 1: Research projects approved in 2004

Class	Max.Point	Application	# of Proj.	Total points			
				Applied		Approved	
				Sys-A	Sys-B	Sys-A	Sys-B
A	100k	any time	4	200K	200K	200K	200K
B	2M	twice a year	48	67.1M	23.65M	66.1M	23.45M
C	20M	twice a year	93	1044.5M	542.2M	954.3M	508.7M
D	none	any time	6	37M	106M	35M	103M

For System-A 1 K point corresponds to charge for CPU time of about 0.43 hours by one processing element, while the corresponding figure is 2.32 hours for System-B.

Exploration of Ultimately Dense Phase of Dioxide under High Pressure

N. Funamori and T. Yagi

Materials transform to denser phases with increasing pressure. The densest structure of dioxides reported so far is the $PbCl_2$ type in which each cation is surrounded by 9 oxygens (9-fold coordinated). Many dioxides with large cations are known to have the $PbCl_2$ structure under high pressure, but any phase transformation to the structure with a coordination number of 10 or higher, namely the post-$PbCl_2$ structure, has not been reported. The purpose of this study is to explore the post-$PbCl_2$ transformation of dioxides. Since lead is in the same group of carbon and silicon and PbO_2 is known to have the $PbCl_2$ structure under high pressure [1], CO_2 and SiO_2, which are important compounds in Earth & Planetary Physics, may have the $PbCl_2$ and/or the post-PbCl2 structure at ultimately high pressures (for example, inside the giant planets). At present, pressures above 100~200 GPa are not easy to achieve in static-compression experiments. Since there is an inverse correlation between cation radius and transition pressure, it is better to choose a dioxide with a larger cation to explore the post-$PbCl_2$ transformation in a limited pressure range. We chose TeO_2whose cation radius is larger than those of dioxides reported to have the $PbCl_2$ structure, such as CeO_2, TiO_2, ZrO_2, HfO_2, and PbO_2 [e.g.1 - 3].

In this study, phase transformations of TeO_2 have been investigated up to 150 GPa using the diamond-anvil cell. TeO_2 (paratellurite, 6-fold coordinated) powder was loaded in a rhenium gasket without pressure medium and compressed to a target pressure and then heated using Nd:YAG laser to anneal deviatoric stresses and/or to overcome kinetic barriers to transformations. The sample itself absorbed the laser beam. Angle-dispersive synchrotron X-ray diffraction experiments were carried out using an imaging-plate detector at BL-13A and BL-18C of the Photon Factory (Tsukuba, Japan). All measurements were conducted at room temperature after heating.

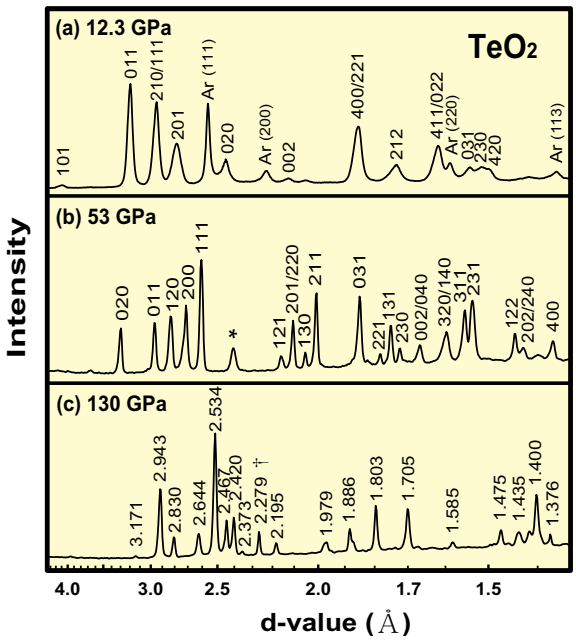

Fig. 1. X-ray diffraction patterns of TeO_2 for (a) the paratellurite phase at 12.3 GPa, (b) the $PbCl_2$ phase at 53 GPa, and (c) the post-$PbCl_2$ phase at 130 GPa. The diffraction lines of the paratellurite phase and the $PbCl_2$ phase are labeled hkl Miller indices, assuming P212121 and Pnam symmetries, respectively. Experiments below 20 GPa were carried out with argon pressure medium without laser heating (see text). The diffraction lines of argon are labeled Ar(hkl). Because the structure of the post-$PbCl_2$ phase has not been determined yet, the diffraction lines in (c) are labeled d-values in Å, instead of Miller indices. The diffraction lines with an asterisk (*) and a dagger (†) may be impurity lines.

Fig. 1 shows typical X-ray diffraction patterns for three phases of TeO_2 observed in this study. Our X-ray diffraction measurements confirm the transformation from the paratellurite phase (Fig. 1(a)) to the $PbCl_2$ phase (Fig. 1(b)) that has been inferred from Raman scattering measurements [4] at pressures of 20~30 GPa. A fit of measured pressure-volume data of the $PbCl_2$ phase to the second-order Birch-Murnaghan equation of state gave the zero-pressure bulk modulus K_0 = 115±17 GPa (and the zero-pressure molar volume V_0 = 23.3±0.6 cm^3/mol). This bulk modulus is as small as (or smaller than) about a half of those of other $PbCl_2$-structured dioxides [e.g.1 - 3], implying that the $PbCl_2$ structure of TeO_2 is more sensitive to pressure than the others. This supports our speculation that TeO_2 may transform to a post-$PbCl_2$ phase at relatively low pressures. Indeed, a further transformation to a post-$PbCl_2$ phase (Fig. 1 (c)) has been observed for the first time in dioxides at pressures of about 80~100 GPa. The X-ray diffraction pattern of the post-$PbCl_2$ phase of TeO_2, however, could not be explained by assuming the post-$PbCl_2$ structures reported in dihalides such as the Co_2Si and Ni_2In structures [5, 6], and the nature of this phase has not been clarified yet. The $PbCl_2$ phase of TeO_2 contracted rather isotropically with increasing pressure similar to other dioxides [1, 3], in marked contrast with the anisotropic contraction of the $PbCl_2$ phases of dihalides [5, 6]. These results suggest that the mechanism of the post-$PbCl_2$ phase transformation in dioxides may be different from that in dihalides.

References

[1] J. Haines, J. M. Leger, and O. Schulte, J. Phys.: Condens. Matter **8**, 1631 (1996).
[2] S. J. Duclos *et al*., Phys. Rev. B **38**, 7755 (1988).
[3] N. A. Dubrovinskaia *et al*., High Pressure Research **22**, 391 (2002).
[4] A. Jayaraman and G. A. Kourouklis, Pramana-J. Phys. **36**, 133 (1991).
[5] J. M. Leger *et al*., Phys. Rev. B **52**, 13247 (1995).
[6] J. Haines, J. M. Leger, and O. Schulte, Phys. Rev. B **57**, 7551 (1998).

Authors
N. Funamori[a], T. Sato[a], T. Yagi, and N. Miyajima
[a] Department of Earth and Planetary Science, University of Tokyo

Organic Semiconductor with Divalent BEDT-TTF Molecules

H. Ito and H. Tajima

The BEDT-TTF [bis(ethylenedithio)tetrathiafulvalene] molecule has been widely used as a constituent of conducting and superconducting cation-radical salts. It is widely believed that in order to realize electrical conduction in BEDT-TTF salts, incomplete charge transfer between BEDT-TTF and appropriate acceptors is important so as to have an intermediately-filled conduction band comprised of overlapping highest-occupied molecular orbitals (HOMO) of the BEDT-TTF molecules. Recently, Kanehama *et al.* reported the rather high conductivity of 10^{-2} S/cm in (BEDT-TTF)Cu_2Br_4. Figure 1 shows the temperature dependence of conductivity. The conductivity shows thermally activated behavior with activation energy of 0.16 eV

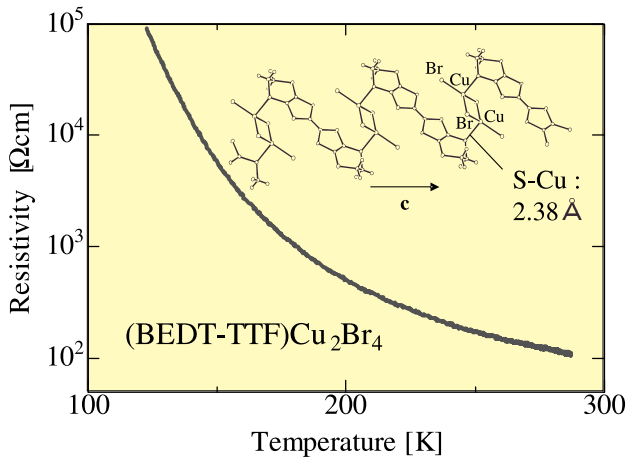

Fig. 1. The temperature dependence of the resistivity of (BEDT-TTF)Cu_2Br_4. Inset: the chain structure of BEDT-TTF^{2+} and $Cu_2Br_4^{2-}$.

below 170 K and 0.09 eV above 170 K. This salt attracts interest in the sense that the valence state of BEDT-TTF is considered to be 2+, because Cu ions are monovalent found by ESR measurements. There are only few preceding examples of salts with divalent BEDT-TTF, (BEDT-TTF)$(BF_4)_2$ and (BEDT-TTF)$(ClO_4)_2$, and more recently (BEDT-TTF)$[Fe(CN)_4(CO)_2]$, but they are all insulators with conductivities less than 10^{-5} S/cm. The good electrical conductivity of (BEDT-TTF)Cu_2Br_4 contradicts to the closed-shell state of BEDT-TTF with no electrons in the HOMO band. It is noted that the S atoms of the BEDT-TTF molecules are coordinated directly to the Cu atoms of the anion clusters with a bond length of 2.38 Å, forming a chain structure along the *c*-axis as shown in the inset of Fig.1.

Figure 2 shows the Raman spectrum under He-Ne Laser excitation, polarized perpendicular to the *c*-axis at room temperature. Among the observed Raman signals, ν_2, ν_3, ν_5, ν_6, ν_7, and ν_9 can be assigned to major a_g mode molecular vibrations of BEDT-TTF. The a_g mode molecular vibrations are known to be sensitive to the charge concentration on HOMO of BEDT-TTF. In the present salt, these are observed at 1383, 1310, 1298, 943, 916, and 530 cm^{-1}, respectively. These Raman shifts are in good agreement with the results for the divalent salt of (BEDT-TTF)$(ClO4)_2$ [2], indicating that the present salt is composed of divalent BEDT-TTF molecules. The Raman spectrum is almost unchanged with temperature down to 20 K, indicating that the valence state of BEDT-TTF remains divalent down to 20 K. The optical

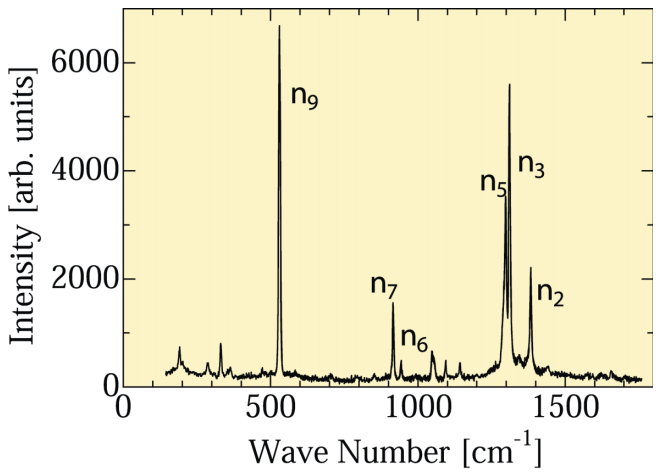

Fig. 2. Raman spectrum at room temperature of a single crystal of (BEDT-TTF)Cu_2Br_4 under He-Ne laser excitation, polarized perpendicular to the *c*-axis.

conductivity of (BEDT-TTF)Cu_2Br_4 exhibits a semiconducting behavior with the electronic gap of 0.7 eV, which contradicts to the low activation energy found by the conductivity measurement. This implies that (BEDT-TTF)Cu_2Br_4 is an extrinsic semiconductor.

In order to obtain insights into the origin of the charge carriers, the Hall coefficient and π-electron ESR measurements were performed [3]. By the Hall coefficient measurement, charge carriers are electron-like and their concentration is rather low of $4\pm2\times10^{19}$ /mol at room temperature. The carrier concentration increases exponentially with temperature with an activation energy of 0.17 eV below 170 K and 0.12 eV above 170 K. The Hall mobility is as high as 2 cm^2/Vs, supporting the high conductivity of the salt. The carrier concentration at room temperature is one order of magnitude lower than the concentration of Curie spin from impurity sites. The fine structure of the ESR signal of Curie spins smears away above 100 K, as caused by exchange interaction mediated via conduction electrons. These results indicate that charge carriers localized at low temperatures are thermally activated to the conduction band at high temperatures to contribute to the conduction. The possible origins of the charge carriers are impurity sites of the different crystal phases of (BEDT-TTF)$_2$[Cu_4Br_6(BEDT-TTF)] in the matrix.

References
[1] R. Kanahama *et al.*, Inorg. Chem. **42**, 7173 (2003).
[2] H. H. Wang *et al.*, Mol. Cryst. Liq. Cryst. **284**, 211 (1996).
[3] H. Ito *et al.*, Phys. Rev. B **71**, 085202 (2005).

Authors
H. Ito[a], Y. Yokochi[a], H. Tanaka[a], S. Kuroda[a], R. Kanehama[b], M. Umemiya[b], H. Miyasaka[b], K-I. Sugiura[b], M. Yamashita[b], H. Tajima, and J. Yamaura
[a] Department of Applied Physics, Nagoya University
[b] Department of Chemistry, Tokyo Metropolitan University and CREST

Novel Technique for Thermal Conductivity Measurements for Organic Materials and the Thermal Conductivity of $(DMe\text{-}DCNQI)_2Li_{1-x}Cu_x$ ($0 \leqq x \leqq 1$)

K. Torizuka and H. Tajima

Organic molecular conductors have recently attracted the interest of many researchers in condensed matter physics. In order to explore the properties of organic compounds, so far electrical conductivity, susceptibility and NMR measurements have been mainly carried out. Other measuring techniques have been little used for organic samples. This is because organic materials are in general so small and fragile that it is very difficult to manipulate. Many researchers have today expected that a new technique should be put into practice in the research field of organic materials. With such situation, we paid our attention to the thermal conductivity measurement. We have developed a new technique to measure the heat conduction for organic samples.

What is new in our technique is the installation of two heaters and three thermometers unlike the conventional technique. Our method takes into account the heat leak through electrical leads. We apply a heat pulse twice. By first application of the heat Q, the heat flows both through the sample and through the leads, i.e.,

$$Q = (\Delta T)\kappa_1 + (\Delta T_0)\kappa_2$$

where κ_1 and κ_2 are thermal conductivities of the sample and

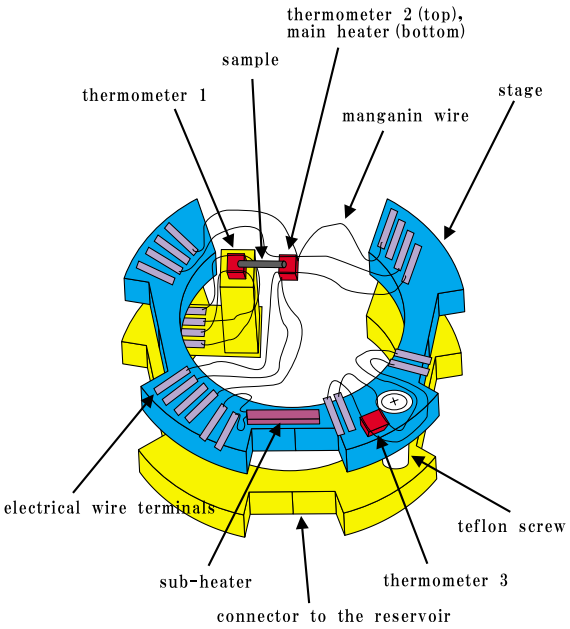

Fig. 1. Actual experimental setup.

the leads, respectively, and ΔT and ΔT_0 are temperature differences across the sample and across the leads, respectively. Then we excite the sub-heater that is installed on a copper stage to which all electrical leads coming from thermometers and the main heater are thermally anchored, and thus we can change the copper stage temperature slightly(≦0.8 K). Under this condition, we apply second heat Q, which again flows both through the sample and through the leads, i.e.,

$$Q = (\Delta T')\kappa_1+(\Delta T_0')\kappa_2$$

where the temperature differences across the sample and across the leads are varied to $\Delta T'$ and $\Delta T_0'$, respectively. By solving these two equations, we can obtain the thermal conductivities κ_1 and κ_1. This is the basic concept of our measurements. The actual setup is sketched in Fig. 1. We can measure the heat conduction over a wide range of temperatures (4≦T≦250K). The resolution of our method is ~1.0×10^{-6} W/K, that is very sensitive. The details of our apparatus have been described elsewhere [1].

The temperature dependences of the thermal conductivity of spin Peierls organic materials $(DMe\text{-}DCNQI)_2Li_{1-x}Cu_x$ (x=0, 0.08, and 0.14) are depicted in Fig. 2. We observed the phonon contribution in the whole range measured. A phonon peak can be seen near 20 K. This peak denotes a crossover between the phonon mean free path that diverges as T^{-2} and the phonon specific heat that decreases as T^3. The peak

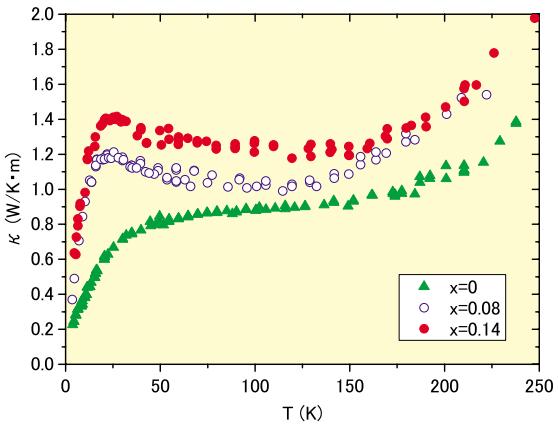

Fig. 2. The thermal conductivity vs. temperature of the $(DMe\text{-}DCNQI)_2Li_{1-x}Cu_x$ (0≦x≦0.14).

height decreases with decreasing Cu concentration x, and finally vanishes in the x=0 sample. We have proposed the phonon scattering mechanism that the spin Peierls lattice distortion may suppress the phonon propagation. We have discussed the effect of the spin Peierls lattice distortion on the phonon propagation for the first time [2].

We have measured the thermal conductivity of x=1 and x=0.75 samples as well, which are metals and are classified into a different class from samples of 0≦x≦0.14. Physical interpretations on experimental data are now in progress.

References
[1] K. Torizuka *et al.*, Rev. Sci. Instrum. **76**, 033908 (2005).
[2] K. Torizuka *et al.*, Phys. Rev. B **71**, 193101 (2005).

Authors
K. Torizuka, H. Tajima, T. Yamamoto[a]
[a] Institute for Molecular Science

Giant Nonlinear Conduction in the Organic Salt θ-$(BEDT\text{-}TTF)_2CsZn(SCN)_4$

I. Terasaki and H. Mori

Very recently, "intrinsically inhomogeneous" states have attracted a keen interest in strongly-correlated electron systems. A prime example is high-temperature superconductors, in which nano-size domains of the superconducting-gap and pseudo-gap phases coexist in the CuO_2 plane [1]. Another example is perovskite manganites, in which percolation paths of the ferromagnetic metal phase give rise to colossal magnetoresistance effects [2]. These nano-scale inhomogeneities are driven by competing orders, not by imperfections of the crystal, hence the name "intrinsic inhomogeneity" [3].

We have discovered giant nonlinear conduction in the organic salt θ-$(BEDT\text{-}TTF)_2CsZn(SCN)_4$, which can be ascribed to a brand-new phenomenon of intrinsically inhomogeneous states [4]. This salt is a layered material composed of conducting BEDT-TTF layers and insulating

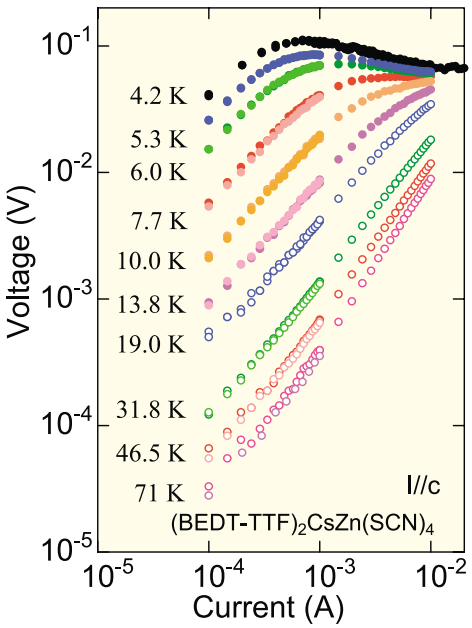

Fig. 1. The voltage-current characteristics of the organic salt θ-$(BEDT\text{-}TTF)_2CsZn(SCN)_4$. The current is applied along the *c*-axis direction (along the conducting BEDT-TTF plane). Note that negative derivative resistance like a thyristor appears below 6 K for 1 mA < I < 10 mA.

$CsZn(SCN)_4$ layers alternately stacked along the *b* axis. The Greek letter θ specifies a packing pattern of BEDT-TTF molecules in the conducting layer, representing a "triangular lattice" Because of charge frustration on the triangular lattice, two kinds of charge order compete at low temperatures. They are eventually frozen as nano-size domains without long range order. In fact, no jump or cusp is detected in either the specific heat or the susceptibility.

Figure 1 shows the voltage-current (*V-I*) characteristics of the present salt. The current is applied along the c-axis direction (along the conducting BEDT-TTF plane). The *V-I* characteristics are highly nonlinear below 10 K. In particular, negative derivative resistance appears below 6 K for 1 mA < I < 10 mA, behavior normally associated with thyristor devices. In this sense, we may call the θ-salt an "organic thyristor".

The most important finding is that the nonlinear conduction is realized *without any thermodynamic transitions*. This is in stark contrast to a charge-density-wave (CDW) conductor, in which the conduction is ohmic above the transition temperature T_c but becomes highly nonlinear (sliding motion of CDW) *below* T_c. The CDW transition with long range order is indispensable in this case.

We have ascribed the data in Fig. 1 to melting of the charge-order domains by an external current. This is a non-equilibrium thermodynamic phenomenon in which ordered phase domains are melted by an external steady flow. On a cold wintry day, we often see ice on a pond and water flowing in a river. The present result is a manifestation of such phenomena in a sea of conduction electrons.

References

[1] K. M. Lang *et al.*, Nature **415**, 412 (2002) .
[2] M. Uehara *et al.*, Nature **399**, 560 (1999).
[3] J. Burgy *et al.*, Phys. Rev. Lett. **87**, 277202 (2001).
[4] K. Inagaki, I. Terasaki, H. Mori and T. Mori, J. Phys. Soc. Jpn. **73**, 3364 (2004) and references therein.

Authors

I. Terasaki[a], M. Abdel-Jawad[b], N. E. Hussey[b], F. Sawano[a], H. Mori, and T. Mori[c]
[a] Waseda University
[b] University of Bristol
[c] Tokyo Institute of Technology

Exact Calculation of Correlation Functions for the Spin-1/2 Anti-Ferromagnetic Heisenberg Chain

H. E. Boos and M. Takahashi

The anti-ferromagnetic spin-1/2 Heisenberg chain $H = J \sum_{j=1}^{L} \mathrm{S}_j \cdot \mathrm{S}_{j+1} \quad (J > 0)$ is one of the most fundamental models in the study of quantum magnetism in low dimensions. The eigenvalues and the eigenfunctions of the system especially for the ground state were obtained by Bethe ansatz, which allowed us to calculate many physical quantities exactly [1]. However, as for the exact analytic evaluation of the correlation functions, it has not been solved fully yet, although there are rapid developments recently. For example, the exact results for the two-point spin-spin correlators in the ground state in the thermodynamic limit ($L \to \infty$) had been known only for the nearest-neighbor $\langle \mathrm{S}_j \cdot \mathrm{S}_{j+1} \rangle = 1/4 - \ln 2$ and the second-neighbor $\langle \mathrm{S}_j \cdot \mathrm{S}_{j+2} \rangle = 1/4 - 4\ln 2 + 9/4\,\zeta(3)$ ones for a long time [1].

Here $\zeta(s)$ is the Riemann zeta function. It was quite recently that Sakai *et al* [2] succeeded in calculating the third-neighbor correlator

$$\langle \mathrm{S}_j \cdot \mathrm{S}_{j+3} \rangle = \frac{1}{4} - 9\ln 2 + \frac{37}{2}\zeta(3) - 14\zeta(3)\ln 2 - \frac{9}{2}\zeta(3)^2 - \frac{125}{8}\zeta(5) + 25\zeta(5)\ln 2$$

by evaluating the relevant multiple integral formulas using the method in [3]. More recently a different but more efficient way to calculate the correlation functions has been devised in [4] based on the quantum Knizhnik-Zamolodchikov equations. We have generalized this new method further and succeeded in calculating all the correlation functions among five lattice sites. In particular, the fourth-neighbor correlator was obtained as [5]

$$\langle \mathrm{S}_j \cdot \mathrm{S}_{j+4} \rangle = \frac{1}{4} - 16\ln 2 + \frac{145}{2}\zeta(3) - 162\zeta(3)\ln 2 - \frac{879}{4}\zeta(3)^2 - \frac{875}{4}\zeta(5) + 1450\zeta(5)\ln 2 - \frac{825}{16}\zeta(3)\zeta(5) - \frac{5625}{16}\zeta(5)^2 + \frac{9555}{64}\zeta(7) - \frac{5145}{4}\zeta(7)\ln 2 + \frac{19845}{32}\zeta(3)\zeta(7)$$

Thus nowadays, it is no more a dream to obtain the exact analytic expressions for the correlation functions for the anti-ferromagnetic Heisenberg chain. In fact, more and more new results are being reported successively [6].

References

[1] M. Takahashi, *Thermodynamics of One-Dimensional Solvable Models* (Cambridge University Press, Cambridge 1999).
[2] K. Sakai, M. Shiroishi, Y. Nishiyama, and M. Takahashi, Phys. Rev. E **67**, 065101 (2003).
[3] H. E. Boos and V. E. Korepin, J. Phys. A: Math. Gen. **34**, 5311 (2001).
[4] H. E. Boos, V. E. Korepin, and F. A. Smirnov, Nucl. Phys. B **658**, 417 (2003).
[5] H. E. Boos, M. Shiroishi, and M. Takahashi, Nucl. Phys. B **712**, 573 (2005).
[6] J. Sato and M. Shiroishi, J. Phys. A: Math. Gen. **38**, L405. (2005).

Authors

H. E. Boos[a], M. Shiroishi, and M. Takahashi
[a] University of Wuppertal

Magnetic "Ice-Order" in Honeycomb Nano-Network of Permalloy Wire

H. Miyajima and Y. Iye

Control of magnetic domain structure is one of the key ingredients of the study of magnetic nanostructures with possible application to future data storage devices and spintronic functionality devices. In this work we have studied the magnetic domain configuration and magnetization process in magnetic nanostructure with geometrical frustration.

Samples of permalloy ($Ni_{81}Fe_{19}$) wire network with honeycomb pattern were fabricated by electron-beam lithography followed by electron-beam evaporation and lift-off process (Fig.1(a)). The magnetic domain pattern of the network was investigated by a magnetic force microscope (MFM) observation. Magnteoresistance measurements were performed in a vector magnet system which enabled us to control the in-plane and out-of-plane components of applied magnetic field and also the azimuthal angle of the in-plane field with respect to the probe current.

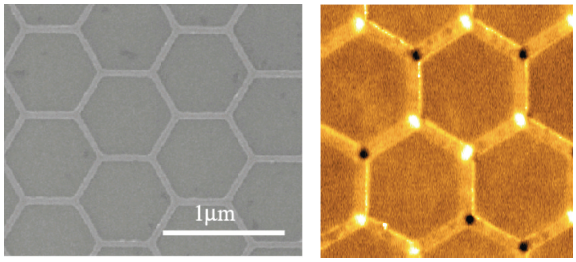

Fig.1. (a) Scanning electron micrograph of the permalloy honeycomb network. (b) Magnetic force microscope (MFM) image of the network, the bright and dark spots at the vertices reflect the stray field emanating there.

Figure 1(b) shows the MFM image of the network in a remanent state after application of $\mu_0 H_\perp$=1T. The individual wire segments are expected to be of single domain with magnetization oriented parallel to the wire due to the shape anisotropy. The bright and dark spots seen at the vertices testify that this is indeed the case, and that the domain configuration of the three wire segments differs from vertex to vertex. In general, there are four possible configurations, *i.e.* "three-in", "two-in/one-out", "one-in/two-out", and "three-out". However, it was found that all the bright and dark spots are roughly equal in magnitude, which means that only two of the above four possible configurations are present in reality. The fact that some of the wire segments have the same bright (or dark) spots on both ends, rules out the possibility of these spots being "three-in" or "three-out". Thus the configuration at each vertex must be either "two-in/one-out" or "one-in/two-out". Since there are three possible choices of the "one" for each of these configurations, the total number of possible configurations at each vertex is six. This is an analog of the so-called "ice-rule", and this leads to a large degeneracy in the magnetization configuration of the total system. The problem can be mapped onto an Ising spin model on a kagome lattice.

The magnetization process of the honeycomb network was traced by magnetoresistance measurements. Figure 2(a) shows the magnetoresistance as a function of the parallel field $H_\parallel$ oriented to θ=75° with respect to the direction of the probe current, in the absence of perpendicular field. The abrupt jumps in resistance correspond to rapid reversal of the wire segment magnetization. In this case as well as in the absence of the perpendicular field, only two abrupt jumps occur in the course of the $H_\parallel$-sweep, despite that there exist three non-equivalent orientations of the wire segments with respect to $H_\parallel$. This behavior suggests that the ice-rule dictates the magnetization process and the remanent state. Namely, in this case, the magnetization reversal of the three inequivalent wire segments are not independent from each other because of the prohibition of the "three-in" and "three-out" configurations.

Figure 2(b) shows a similar trace taken while a slightly stronger perpendicular field ($\mu_0 H_\perp$= 0.4T) is applied. In this case, three discontinuities are observed, indicating that the constraint by the ice-rule is lifted. In the presence of perpendicular magnetic field, the magnetic energy at the vertices are reduced, so that the energy differences between the "three-in" or "three-out" and the other two configurations becomes smaller, making the former two configurations accessible.

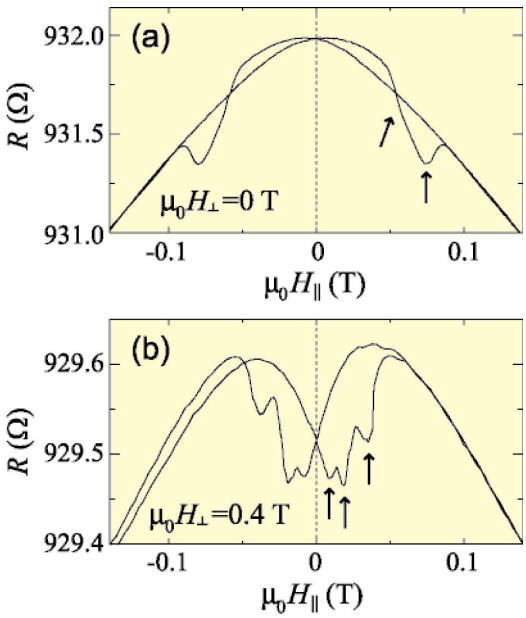

Fig.2. (a) Magnetoresistance trace as a function of the parallel field $H_\parallel$ in the absence of perpendicular field, showing two jumps. (b) Similar trace with $\mu_0 H_\perp$=0.4T showing three jumps.

Reference

[1] M. Tanaka, E. Saitoh, H. Miyajima, T. Yamaoka, and Y. Iye, J. Appl. Phys. **97**, 10J710 (2005).

Authors
M.Tanaka[a], E.Saitoh[a], H.Miyajima[a], T.Yamaoka[b], and Y.Iye
[a] Department of Physics, Keio University
[b] SII NanoTechnology Inc.

STM and AFM; Which is better for Surface Structural Analysis? Non-contact AFM Studies on Ge/Si(105) Surface

Y. Hasegawa and T. Sakurai

Scanning tunneling microscopy (STM) has been utilized to determine surface atomic structure with its atomically

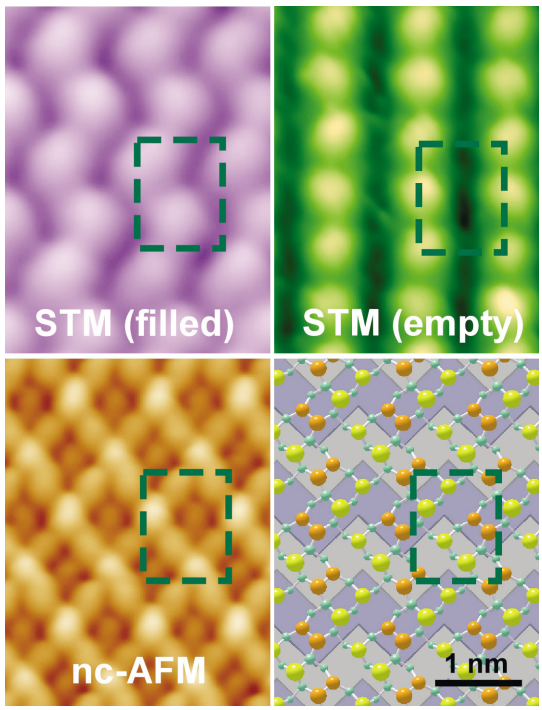

Fig. 1. Filled-state STM, empty-state STM and nc-AFM images of the Ge(105)-(1×2) surface and its structural model. The (1×2) unit cell (1.39 nm × 1.08 nm) is depicted at an identical position in each figure.

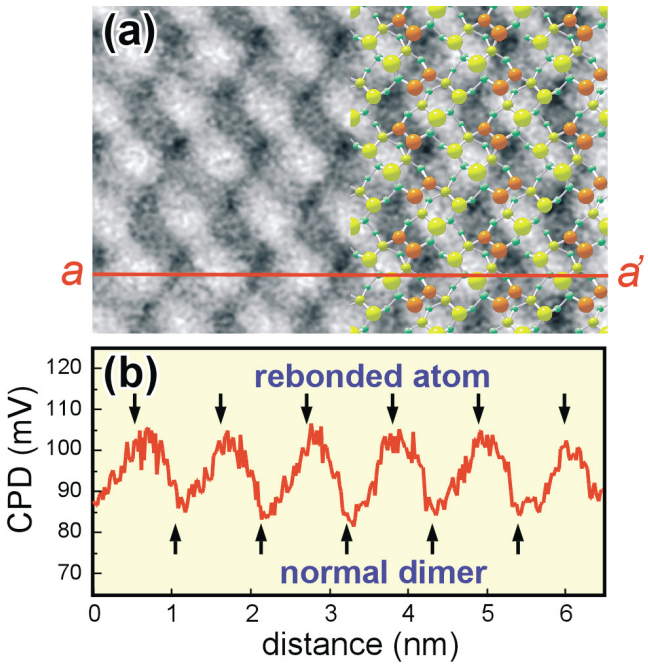

Fig. 2. Electrostatic potential mapping (a) and profile (b) taken on the Ge/Si(105) surface.

resolved images. Probing surface electronic states near the Fermi energy, STM images, however, do not necessarily represent the atomic structure of surfaces. It has been naively believed that atomic force microscopy (AFM) provides us with surface topographic images without being disturbed by the electronic states. In order to demonstrate the possibly unique property of AFM, we performed non-contact AFM (nc-AFM) studies on the Ge/Si(105) surface [1], which is a facet plane of the nano-size "hut" clusters formed on Ge-deposited Si(001) surface.

As presented in Fig. 1, neither filled-state images nor empty-state images of STM shows all surface atoms. This is due to the fact that the atoms observed in the filled-state image, called normal dimer atoms and colored yellow in the structural model, have dangling bond states below the Fermi energy (E_F) while the atoms in the empty-state image, called rebonded atoms and colored orange in the model, have states above E_F [2]. On the other hand, in a nc-AFM image all surface atoms having a dangling bond are clearly observed, directly representing an atomic structure of the surface.

Atomically resolved AFM images are realized by detecting a covalent bonding between the surface and tip apex atoms [3]. When dangling bonds are tilted from the surface normal, thus, the observed atom position should be shifted from its core in AFM images. The slight difference in the atomic positions between the model and AFM image is explained with the tilted dangling bonds.

Electronic information can also be obtained in AFM by using a Kelvin-probe method. From atomically resolved potential profile obtained with Kelvin-probe force microscopy, charge transfer among the dangling bond states is directly observed.

These results clearly demonstrate that highly-resolved nc-AFM with the Kelvin-probe method is an ideal tool for analysis of atomic structures and electronic properties of surfaces, surpassing STM.

References

[1] T. Eguchi, Y. Fujikawa, K. Akiyama, T. An, M. Ono, T. Hashimoto, Y. Morikawa, K. Terakura, T. Sakurai, M.G. Lagally, and Y. Hasegawa, Phys. Rev. Lett. **93**, 266102 (2004).
[2] Y. Fujikawa *et al*., Phys. Rev. Lett. **88**, 176101 (2002).
[3] T. Eguchi and Y. Hasegawa, Phys. Rev. Lett. **89**, 256105 (2002).

Authors
T. Eguchi, Y. Fujikawa[a], K. Akiyama, T. An, M. Ono, T. Hashimoto[b], Y. Morikawa[c], K. Terakura[d], T. Sakurai[a], M.G. Lagally[e], and Y. Hasegawa,
[a] Institute for Materials Research, Tohoku University
[b] Research Institute for Computational Sciences, AIST
[c] The Institute of Scientificand Industrial Research, Osaka University
[d] Creative Research Initiative, Hokkaido University
[e] University of Wisconsin-Madison

Dynamics of Super Spin and Mass Currents in ^{3}He-A_1

H. Kojima and H. Ishimoto

When liquid ^{3}He is cooled in a magnetic field to low enough temperatures, the normal liquid first makes a transition into superfluid A_1 phase at T_{c1} and then into superfluid A_2 phase at a lower temperature T_{c2}. The most important aspect of the A_1 phase is that its superfluid component is totally spin-polarized along the magnetic field. It is a kind of ferromagnetic superfluid. A mass superflow is then simultaneously a spin flow. The phase transition into the A_1 phase is accompanied by the spontaneous breaking of relative spin-gauge symmetry. Interesting hydrodynamic effects occur in the A_1 phase such as a unique magnetic fountain pressure effect which was predicted by Liu and established by Kojima. Nevertheless earlier experiments on this interesting magnetically driven superflow have uncovered puzzling problems. One is the origin of the induced fountain pressure relaxation and the other is the origin of the observed abrupt change in the relaxation time near the middle of the A_1 phase. To clarify these, the magnetic fountain detector should be placed in the sample cell containing only A_1 phase liquid without the interfaces with any other superfluid and normal phase. To realize such conditions, the ISSP nuclear refrigerator with a large experimental space and a high magnetic field capability up to 15 T has been assigned as a US-Japan (NSF-JSPS) joint scientific program. Experimentally a pulsed magnetic field gradient was applied across a superleak between two chambers, and then the accompanied pressure increase and relaxation was measured

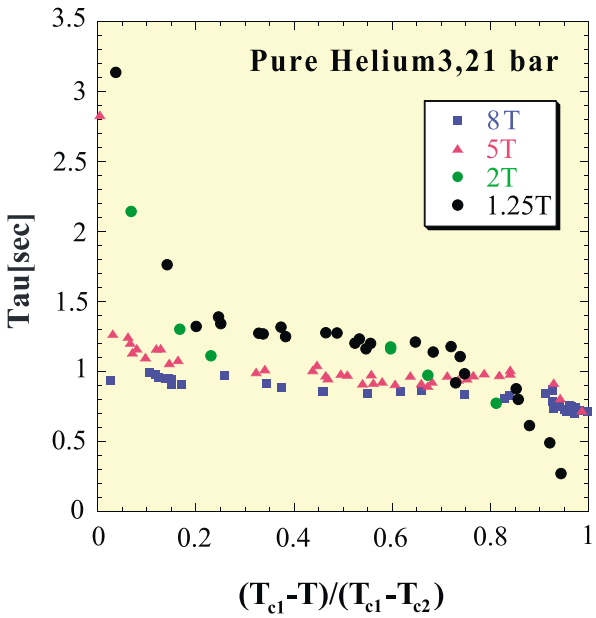

Fig. 1. Relaxation time as a function of reduced temperature (t= (T_{c1} - T)/(T_{c1} - T_{c2})).

with a sensitive differential pressure sensor over the entire magnetic field and pressure region of the A_1 phase. Figure 1 is one of the typical results. Relaxation time (τ) is given as a function of normalized reduced temperature ($t = (T_{c1} - T)/(T_{c1} - T_{c2})$) at 5 and 8 T. No abrupt change is observed near t~0.5, confirming a Grabinski's hypothesis on the effect from the interfacial boundary against the A_2 and the normal phase. As for the pressure dependence, there is a substantial decrease in τ at t=0.5 with increasing the pressure from zero to 30 bar. No or small magnetic field dependence has also observed above 1.5 T, compared with a linear increase in the low field region below 1.0 T. To understand the observed phenomena and to realize a "spin filter" experiment in the A1 phase, further endeavor including the regulation of the sample cell wall is now under way.

References
[1] R. Masutomi, H. Kojima, K. Kimura, A. Yamaguchi, and H. Ishimoto, J. Low Temp. Phys. **138**, 789 (2005).

Authors
H.Kojima[a], R.Masutomi[a], K.Kimura, S.Kobayashi, A.Yamaguchi, and H.Ishimoto
[a] Rutgers University, Picataway, NJ 08854, U.S.A.

Aharonov-Bohm Effect in Aligned Single-walled Carbon Nanotubes

H. Yokoi, K. Uchida, and S. Takeyama

Aharonov-Bohm effect on the quantum states in single-walled carbon nanotubes (SWNTs) is expected to cause lifting of degeneracy in the energy bands of an electron in

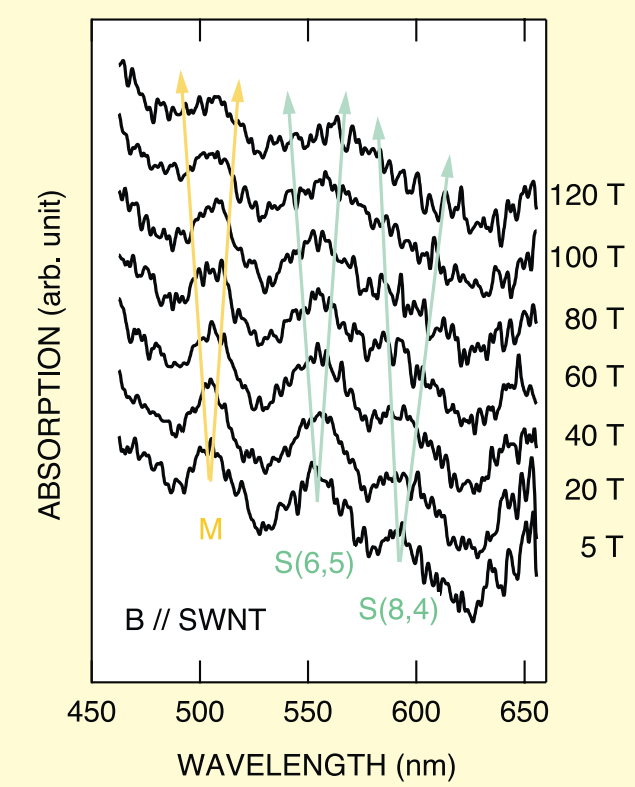

Fig. 1. Magnetic field expansion of absorption spectra of the stretch-aligned SWNTs film in the Voigt configuration with magnetic fields and light polarization parallel to the SWNTs alignment. The symbols M and S are corresponding to metallic SWNTs and semiconducting SWNTs. The chiralities are also shown for the semiconducting SWNTs. Arrows are the guide to the eye indicating field-induced splitting.

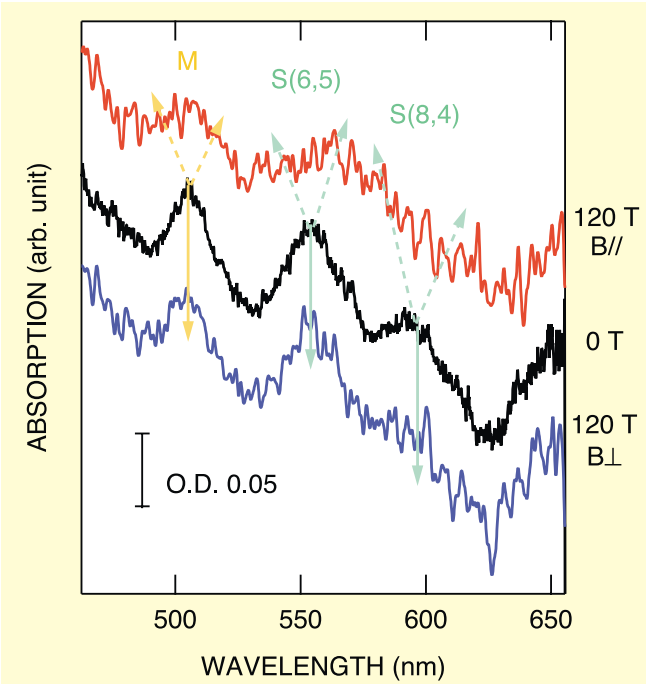

Fig. 2. Comparison of magnetoabsorption spectra of the stretch-aligned SWNTs film between the configurations B parallel and B perpendicular to the alignment of SWNTs at 120 T together with a spectrum at zero field.

SWNTs (Ajiki-Ando splitting)[1]. Recently, absorption and photoluminescence in micelle-suspended SWNTs were measured at magnetic fields to 45 T, and the splitting in the first band gaps of semiconducting SWNTs was found to be almost in line with the Ajiki-Ando splitting.[2] However, the splitting was not resolved for the second band gaps because their spectral peak widths are broad, compared to the splitting amount. In addition, magneto-optical effect under magnetic fields applied perpendicularly to the SWNT axis was not examined sufficiently because SWNTs were suspended in water in their experiments. Both experimental proofs are essential in order to make the assignment to the Aharonov-Bohm effect conclusive. Especially, the former phenomenon is important in the viewpoint that level crossing between the first subband and the second is predicted to occur at higher magnetic fields.

We have conducted absorption measurements in stretch-aligned SWNTs films[3] at magnetic fields to 120 T. Well-resolved spectral peaks associated with the second gaps of the semiconducting (6, 5) SWNT and a metallic SWNT, assigned to (7, 7) tentatively, were observed to broaden when the magnetic field was applied parallel to the SWNTs (Fig. 1). No significant modification of the peaks was recognized when the field was applied perpendicularly to the SWNTs (Fig. 2), which supports the consideration that the peak broadening is due to the Aharonov-Bohm effect. The amount of the peak splitting for the semiconducting and metallic SWNTs was estimated at 0.09 and 0.06 eV, respectively, which agrees semi-quantitatively with the Ajiki-Ando splitting, 0.099 and 0.052 eV, respectively. As excitonic effect is not incorporated in their theory, more quantitative review will be required for the precise study of the Aharonov-Bohm phase in SWNTs. In metallic SWNTs, magnetic field driven metal-semiconductor transition is expected due to the Aharonov-Bohm effect. Our observation of splitting in the first gap in a metallic SWNT would show an affirmative possibility of experimental observation of the transition.

References
[1] H. Ajiki and T. Ando, J. Phys. Soc. Jpn. **62**, 1255 (1993).
[2] S. Zaric *et al*. Science **304**, 1129 (2004).
[3] Y. Kim *et al*. Appl. Phys. Lett. **86**, 073103 (2005).

Authors
H. Yokoi[a], N. Kuroda[a], Y. Kim[b], N. Minami[b], S. Kazaoui[b], K. Uchida, and S. Takeyama
[a] Dept. of Mechanical Eng. and Materials Sci., Kumamoto Univ.
[b] Nanotechnology Research Institute, AIST

Vortices in Superfluid ^{3}He Induced by Rotation in Parallel Plate Geometry with 12.5μm Spacing

S. Ishikawa, T. Takagi, T. Mizusaki, and M. Kubota

The Vortex is well known phenomena in nature, for example, tornado and typhoon on the Earth's surface. Vortices in quantum fluids, superfluid ^{3}He and ^{4}He have, however, an interesting feature that circulation of velocity around a core is quantized, with a minimum circulation quantum number possible. When we rotate a bucket filled with water, we observe a single vortex with continuously changing strength. It is quite different when we have a superfluid in the bucket. The number of vortices changes according to the rotational speed because each vortex is quantized. Superfluid vortices form cluster or lattice and rotate with the container.

Superfluid ^{3}He has many degrees of internal freedom and also has many types of vortices depending on experimental conditions due to its anisotropic gap structure in the A phase. We put superfluid ^{3}He *A*-phase in parallel plate geometry to study what type of vortex appears by rotation. Stacking parallel plates with holes make many thin disc-shaped spaces with 12.5μm thickness, where superfluid ^{3}He is put in. Spacing of 12.5μm is much longer than the coherence length of the superfluid ^{3}He but is comparable to a healing length on the texture of the order parameter. There are two candidates for vortices in *A*-phase in such a parallel plate geometry. One is called "phase vortex" and the other is "half quantum vortex", which are quite different from vortices in bulk superfluid ^{3}He. Both vortices have been expected to exist in the confined geometry. Our detection method is continuous wave (cw) nuclear magnetic resonance (NMR).

We observed one absorption signal of NMR with negative frequency shift at rest and a satellite signal near the Larmor frequency under rotation (Fig. 1). In Fig. 2, the intensity of satellite signal is plotted as a function of rotational

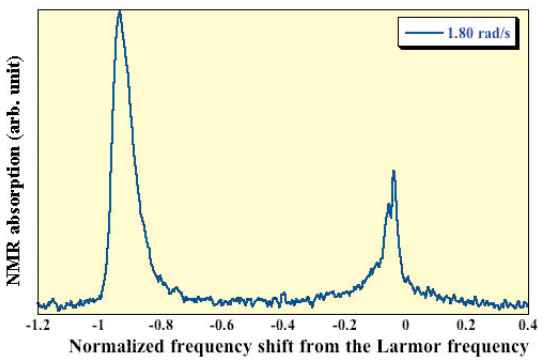

Fig. 1. NMR spectrum at 0.81 T_c. Horizontal line is normalized by the frequency shift of bulk *A*-phase. At 0.01 rad/s, there are the liquid signal of negative shift and the solid signal near the Larmor frequency. At 1.80 rad/s, a spin wave signal appeared near the Larmor frequency.

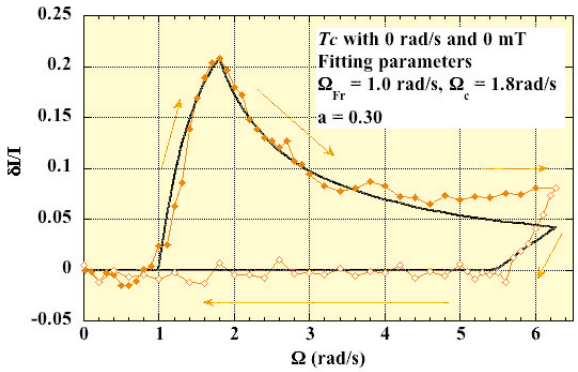

Fig. 2. Increase of the intensity of the spin wave signal *vs*. rotation speed.

speed Ω [rad/s]. As increasing Ω from zero, satellite signal appeared above a threshold value Ω_{Fr} and had maximum value at Ω_c. Further increase of Ω made satellite signal decrease gradually up to our maximum speed Ω_{max}. Appearance of satellite at Ω_{Fr} is attributed to textural transition of order parameter, so called Fréedericksz transition, by the rotation induced counter flow. Our theoretical calculation of texture in parallel plate space under counter flow gives a result that satellite frequency is in agreement with spin wave resonance frequency that is a collectively excited spin motion in a deformed dipole interaction potential by Fréedericksz transition. It should be noted that so far there have been no vortex detected for Ω less than Ω_c. Vortices are formed above Ω_c. We can understand the existence of vortices in parallel plate space by considering reduction of satellite signal intensity. Since vortices form a cluster and give superfluid velocity as a rigid body rotation inside the cluster, the counter flow disappears inside the cluster and decreases outside of it. So these changes of counter flow by vortices give rise to a reduction of satellite signal.

So far the type of vortex in parallel plate is not yet clear. We have not observed any other satellite signal that shows an evidence of soft core vortex as in bulk liquid. This indicates that vortex in parallel plate has singular structure in the vortex core as phase vortex or half quantum vortex is expected to have.

Authors
M. Yamashita[a], K. Izumina, Y. Kataoka, O. Ishikawa[b], T. Takagi[c], Y. Sasaki[a], T. Mizusaki[a,d], and M. Kubota
[a] Department of Physics, Graduate School of Science, Kyoto University
[b] Graduate School of Science, Osaka City University
[c] Department of Applied Physics, Fukui University
[d] Research Center for Low Temperature and Materials Sciences, Kyoto University

Pressure Study of $Ca_3Ru_2O_7$

Y. Yoshida and Y. Uwatoko

Ruddlesden-Popper (R-P) type ruthenates $(Sr, Ca)_{n+1}Ru_nO_{3n+1}$ have attracted many researchers since the discovery of the spin-triplet superconductivity in Sr_2RuO_4 (n=1). Beside the superconductivity, these ruthenates show a wide variety of magnetic and transport properties. In some ruthenates, such as $Sr_3Ru_2O_7$ and Ca_2RuO_4, applying pressure causes drastic changes to their magnetic ground states. Among these R-P type ruthenates, we selected a double-layered Ca-based ruthenate, $Ca_3Ru_2O_7$, showing an anti-ferromagnetic (AF) ordering below 56 K and a first-order transition at 48 K. The crystal structure has the orthorhombic symmetry with *Bb2$_1$m*

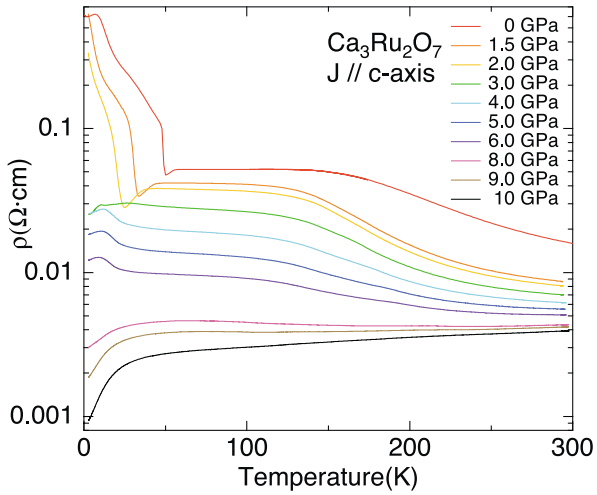

Fig. 1. Temperature dependences of electrical resistivity for the current normal to conducting RuO_2 plane under various pressures.

space group, accompanying both the rotation and tilting of RuO_6 octahedra. The transport property of $Ca_3Ru_2O_7$ is highly anisotropic, and shows a quasi-two-dimensional metal in the ground state.[1] A structural change is accompanied by the first-order transition, where a jump of lattice constant was observed. [2]

In order to investigate the transport and the magnetic properties of $Ca_3Ru_2O_7$ under pressure, we have measured the temperature dependence of the electrical resistivity under high pressure. Applied pressures were up to 10 GPa by using a Cubic anvil apparatus.

Figure 1 shows temperature dependences of the electrical resistivity for the current along c-axis, i.e. normal to conducting RuO_2 plane under various pressures. Both first-order and AF transitions decrease steeply with increasing pressure and vanish around 3GPa. Small peaks around 10 K emerge in the intermediate pressure range. These peaks are almost pressure independent, and do not relate to the transitions at low pressures. The transport property finally changes from insulating to metallic behavior above 8GPa, indicating increase of electron transfer between RuO_2 planes. These results are summarized in a phase diagram, as shown in Fig. 2. The magnetic state in the intermediate region is still unclear so that we need to measure magnetic properties under this pressure range.

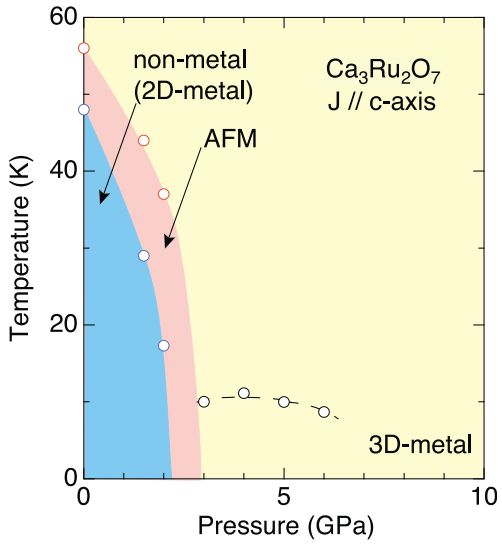

Fig. 2. Phase diagram of $Ca_3Ru_2O_7$

In these metallic region, we have fitted $\rho(T)$ below 10 K to the formula, $\rho(T) = \rho_0 + AT^{\alpha}$. The exponent of α increases from 1.18 to 1.45 with increasing pressure, while the other parameters decrease. This indicates that the metallic behavior of $Ca_3Ru_2O_7$ is approaching that of the Fermi liquid metals with increasing pressure.

References
[1] Y. Yoshida *et al.*, Phys. Rev. B **69**, 220411 (2004).
[2] E. Ohmichi *et al.*, Phys. Rev. B **70**, 104414 (2004).

Authors
Y. Yoshida[a], S. I. Ikeda[a], N. Shirakawa[a], M. Hedo, and Y. Uwatoko
[a] Nanoelectronics Research Institute, National Institute of Advanced Industrial and Technology (AIST)

Discovery of Pressure-Induced Superconductivity in $CeNiGe_3$

M. Nakashima and Y. Uwatoko

High-pressure is useful method to control the magnetic interaction and hybridization between the *f* electrons and conduction electrons. The crossover from the magnetically ordered state to the non-magnetic state under pressure, crossing the quantum critical point, is currently the most interesting issue in cerium compounds. Around the critical pressure, a heavy fermion state or non-Fermi liquid behavior appears at low temperatures. Moreover, superconductivity appears around the critical pressure in some compounds. We have continued in studying the effect of pressure on the cerium and uranium compounds. Among them, we report $CeNiGe_3$ antiferromagnetic Kondo compounds with the orthorhombic structure[1]. To apply high pressures, we used three method, the indenter cell up to 4 GPa, the cubic anvil cell up to 8GPa and diamond anvil cell up to 10 GPa. Polycrystal sample of $CeNGe_3$ was prepared by arc-melting and annealing.

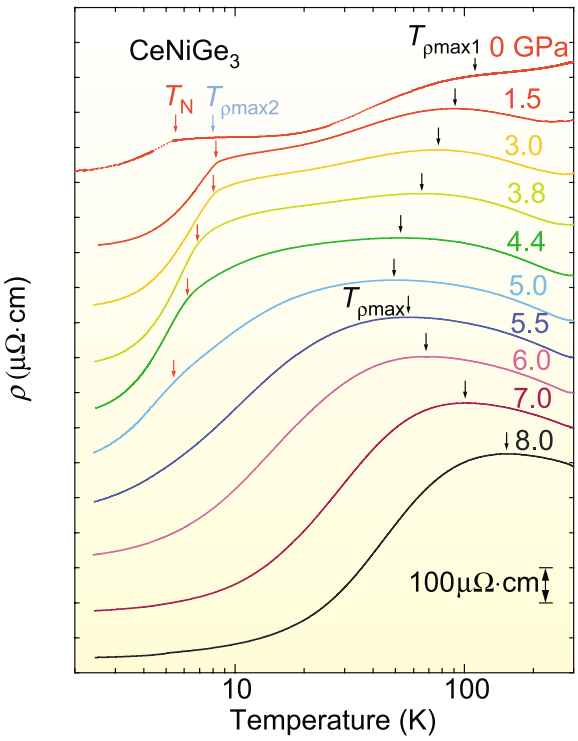

Fig. 1. Logarithmic scale of temperature dependence of the electrical resistivity under pressures in $CeNiGe_3$, which was obtained by using the cubic anvil cell.

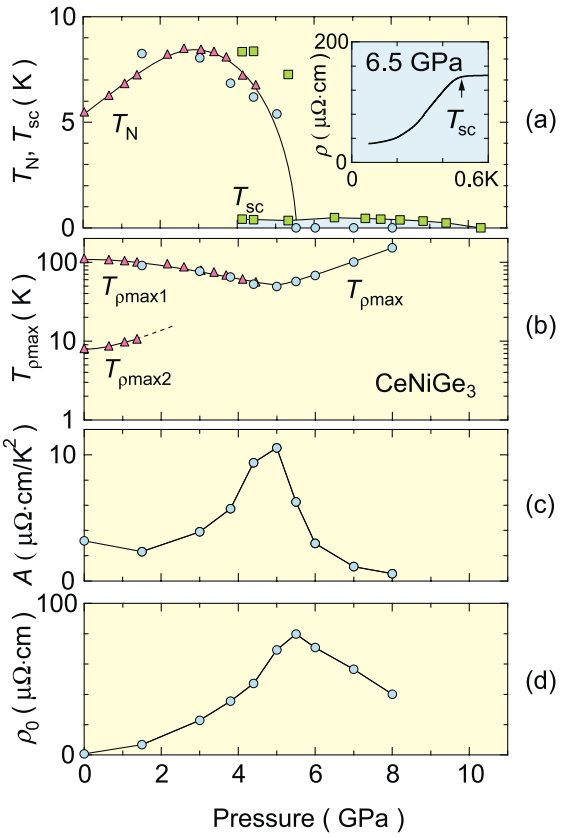

Fig. 2. Pressure dependence of T_N and T_{sc} (a), $T_{\rho max}$ (b), A(c) and ρ_0(d) values in CeNiGe3. The data shown by triangles, circles and squares were obtained by the indenter, cubic and diamond anvil cells, respectively. Inset is the temperature dependence of resistivity at 6.5 GPa.

Figure 1 shows the logarithmic scale of temperature dependence of the electrical resistivity at pressures up to 8.0 GPa in the temperature range of 2 to 300 K, which was obtained by using the cubic anvil cell. The resistivity data at different pressures are arbitrarily shifted downwards for simplicity. The electrical resistivity at ambient pressure has a broad hump around 100 K (=$T_{\rho max1}$) and also a broad peak around 8 K (=$T_{\rho max2}$), and decreases steeply below 5.5 K (=T_N). These are characteristic features in the cerium Kondo compound with antiferromagnetic ordering. The two characteristic features at $T_{\rho max1}$ and $T_{\rho max2}$ are found to merge at 5 GPa into a single resistivity peak at $T_{\rho max}$ = 50K. This single resistivity peak at 5 GPa shifts to higher temperatures with further increasing pressure: $T_{\rho max}$ = 153 K at 8.0 GPa. The antiferromagnetic ordering most likely disappears at 5.5 GPa (=P_c), as shown in Fig. 2(a). The overall temperature dependence of the electrical resistivity around 5-6 GPa are very similar to that in the heavy fermion superconductor $CeCu_2Si_2$[2]. At 8.0 GPa, that is typically similar to that observed in a valence fluctuating compound such as CeNi, where the 4*f* electron is itinerant[3].

We plot the A and $\tilde{\rho}$ values in the Fermi liquid relation of $\rho = \rho_0 + AT^2$ in Fig.2 (c) and (d). The A and ρ_0-values have maximums around P_c . The A value at 5 GPa, 10.5$\mu\Omega$cm is the same as that in $CeCu_2Si_2$ with an extremely large γ-value of 1.1 J/K^{2}mol[2]. The heavy fermion state is thus formed around P_c = 5.5 GPa. In order to look for possible superconductivity around P_c, we measured the low-temperature resistivity by using the diamond anvil cell. Finally, superconductivity is observed in a wide pressure region from 4 to 10 GPa, as shown in inset of Fig. 2. The upper critical field $H_{c2}(0)$ at 6.5 GPa is roughly estimated as 2.0 T[4]. Further studies of superconductivity are now in progress.

References

[1] P. Salamakha *et al.*, J. Alloy. Compd. **236**, 206 (1996).
[2] W. Assumus *et al.*, Phys. Rev. Lett. **52**, 469 (1984).
[3] S. Araki *et al.*, J. Phys. Soc. Jpn. **68**, 3334 (1999).
[4] M. Nakashima *et al.*, J. Phys.: Condens. Matter. **16**, L255 (2004).

Authors

M. Nakashima[a], K. Tabata[b], A. Thamizhavel[a], T. C Kobayashi[c], M. Hedo, Y. Uwatoko, K. Shimizu[b], R. Settai[a], and Y. Onuki[a]

[a] Graduate School of Science, Osaka University
[b] Research Center for Materials Science at Extreme Conditions, Osaka University
[c] Department of Physics, Faculty of Science, Okayama University,

Pressure Effect on Competition between Charge Density Wave and Superconductivity in $ZrTe_3$: Appearance of Pressure-Induced Reentrant Superconductivity

K. Yamaya and Y. Uwatoko

The application of hydrostatic pressure on the low-dimensional conductors generally increases three-dimensionality, leading to depression of the charge density waves (CDW) formation and enhancement of the superconductivity by the restoration of the density of states at the Fermi level. However, unusual pressure dependences of the CDW transition temperature T_{CDW} and the superconducting transition temperature T_C have observed in $ZrTe_3$ which is one of transition-metal trichalcogenides MX_3 that is well known as linear chain compounds, at least up to 1.1 GPa. [1] The CDW formation is enhanced by pressure and the T_{CDW} reaches ~105 K at 1.1 GPa, while the superconductivity is suppressed and the T_C goes down to 1.2 K at 0.5 GPa. A greater pressure is expected to raise the three-dimensionality in $ZrTe_3$. Therefore, it would be very interesting to investigate the pressure dependences of T_{CDW} and T_C at high pressure. We investigated the pressure dependences of T_{CDW} and T_C over a wide pressure range up to 11 GPa using a cubic anvil pressure-cell to discuss a possible existence of competition between the superconductivity and the CDW formation. [2]

Fig. 1 shows the pressure dependence of T_{CDW} and T_C obtained for three samples, together with those for samples measured earlier in the low pressure. As pressure increases, T_{CDW} initially increases, then starts to decrease at ~2 GPa

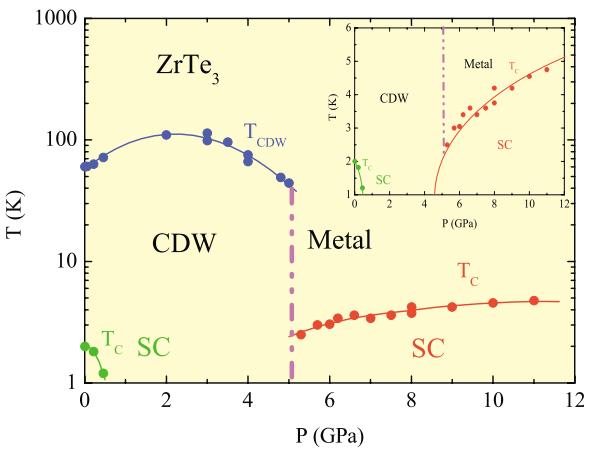

Fig. 1. Pressure dependence of T_{CDW} (closed symbols) and T_C (open symbols) plotted on a logarithmic scale for three samples of $ZrTe_3$. Previous results are also shown at pressure below 1.1 GPa.[1]

and abruptly disappears to below 2.5 K between 5.0 and 5.5 GPa. Thus, CDW of $ZrTe_3$ is sensitive to application of external pressure. On the other hand, T_C decreases with increasing pressure and falls below 1.2 K at ~0.5 GPa. No sign of superconducting transition is observed above 2.5 K in the pressure range of 1.1 – 5 GPa, but the superconducting transition emerges beginning at ~5 GPa. T_C increases steeply with increasing pressure up to 11 GPa. In contrast to the abruptly disappearance of T_{CDW}, the temperature dependence of resistance in the metallic state varies systematically for pressure from 2 to 11 GPa and any anomalous change is not observed around 5 GPa, showing that the abruptly disappearance of T_{CDW} near 5 GPa is not due to a structure phase change. Thus, we conclude that superconductivity observed above 5 GPa is induced by a change in the Fermi surface (FS) under pressure. This is the first observation of pressure-induced reentrant superconductivity. T_C in the pressure range of 0.5 – 5 GPa is shown by extrapolation from the pressure range of $P < 0.5$ GPa and $P > 5$ GPa. The minimum T_C was estimated to be around 2 GPa, where is just a pressure corresponding to the peak of T_{CDW}. Such a remarkable pressure dependent competition between T_{CDW} and T_C has not been reported for other systems of low-dimensional conductors.

Analyzing the size of the resistance anomaly due to the CDW formation, it was found that the intricate competition between CDW and superconductivity is explained by the change in the reduced area of the FS due to CDW formation. A notable feature of the FS of $ZrTe_3$ is the differing dimensionality of quasi-1D, dual quasi-1D+3D and 3D. [3,4] The quasi-1D FS sheets have Te 5px character, while the 3D FS has dominant Zr 4d character. The 1D sheets are responsible for CDW formation, while the dual quasi-1D+3D character is responsible for superconductivity. [3,4] Therefore, the competition between CDW and superconductivity shows the strong hybridization of Te 5px and Zr 4d bands. The detail properties of pressure-induced reentrant superconductivity will be published elsewhere. [5]

References

[1] K. Igarashi, S. Yasuzuka, K. Inagaki, S. Tanda, Y. Okajima, M. Hedo, Y. Uwatoko, and K. Yamaya, J. de Phys. IV **12**, 97 (2002).
[2] R. Yomo, K. Yamaya, M. Abliz, M. Hedo, and Y. Uwatoko, Phys. Rev. B **71**, 132508 (2005).
[3] K. Stowe and F.R. Wagner, J. Solid State Chem. **138**, 160 (1998); C. Felaer, E.W. Frinckh, H. Kleine, F. Rocker, and W. Tremel, J. Matter. Chem. **1**, 1787 (1998).
[4] T.Yokoya, T. Kiss, A. Chainani, S. Shin, and K. Yamaya, Phys. Rev. B**71**, 140504 (2005).
[5] M. Abliz, M. Hedo, Y. Uwatoko, R. Yomo, and K. Yamaya, Phys. Rev. Lett. (in preparation).

Authors

R. Yomo[a], K. Yamaya[a], M. Alibe, N. Hedo, and Y. Uwatoko
[a] Dept. of Appl. Phys., Hokkaido University.

Observation of Two-Photon Above-Threshold Ionization of Rare Gases by XUV Harmonic Photons

S. Watanabe and T. Nakajima

In order to measure attosecond pulses in the extreme ultraviolet (XUV), the observation of single-color two-photon above threshold ionization (ATI) is an important cornerstone toward the "full and direct" characterization of ultrashort pulses in the XUV~soft X-ray range. This is

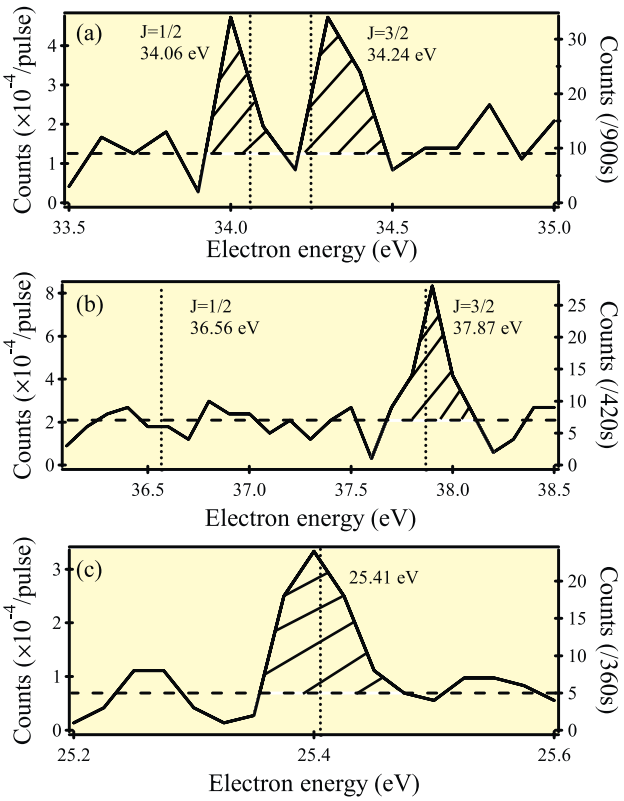

Fig. 1. Photoelectron spectra of two-photon ATI in Ar (a), Xe (b), and He (c).

because (1) for XUV photons even a single-photon absorption will bring atoms above ionization threshold and hence ATI is necessarily involved for any nonlinear processes, and (2) the accuracy of autocorrelation-based pulse measurement has no fundamental limitation in terms of the measurable pulse width. In the shorter wavelength (XUV~soft X-ray), however, we should keep in mind that bright light sources are not easily obtained and the corresponding dipole moments are much smaller than those in the visible~IR range, since large transition energy usually means small overlap of wavefunctions. About the theoretical aspects for the description of two-photon ATI, we are not aware of any calculations which resolve fine structure of the ionic core.

In this study, we report the first experimental observation of single-color two-photon ATI in Ar, Xe, and He in the XUV range at 25 eV photon energy, and compare with our theoretical results. Since the single-color two-photon ATI signal by XUV photons is very weak, a special detection technique is needed. This was realized by the use of the energy-resolved electron counting system at a low repetition rate of 40-100 Hz together with strong 25 eV radiation generated by the 5th harmonic of our KrF/Ti:Sapphire hybrid laser system.

The photon energy of 25 eV is already above the first ionization thresholds of all rare gases. Note that the two-photon absorption of 25 eV photons bring Ar and Xe atoms above the double ionization thresholds. Thus two-photon double ionization as well as two-photon ATI can take place for Ar and Xe. However, the two-photon double ionization cross section is typically about one order of magnitude smaller than that for the two-photon ATI cross section. Besides, the photoelectron spectrum for the two-photon double ionization appears as a background, showing no peak structure. Therefore, it is a natural choice, in particular as a first attempt in the XUV range, to try to observe two-photon ATI. The peaks due to two-photon ATI should

be located at 34.24 eV and 34.06 eV in Ar, 37.87 eV and 36.56 eV in Xe, 25.41 eV in He, respectively.

Figure 1(a) shows the two-photon ATI spectrum of Ar. The two peaks separated by 0.18 eV were resolved. Next the two-photon ATI spectrum of Xe is shown in Fig. 1(b). In Fig. 1(b), only a single peak corresponding to the core of $p^5[^2P_{3/2}]$ was observed. The background noise may have covered the two-photon ATI signal for the $p^5[^2P_{1/2}]$ core. Finally the two-photon ATI spectrum of He is shown Fig. 1(c).

References

[1] N. Miyamoto, M. Kamei, D. Yoshitomi, T. Kanai, T. Sekikawa, T. Nakajima, and S. Watanabe, Phys. Rev. Lett. **93**, 083903 (2004).
[2] T. Nakajima and S. Watanabe, Phys. Rev A **70**, 043412 (2004).

Authors

N. Miyamoto, M. Kamei, D. Yoshitomi, T. Kanai, T. Sekikawa, T. Nakajima[a], and S. Watanabe

[a] Institute of Advanced Energy, Kyoto University

Strain Distributions under the SiO_2/Si(001) Interface Revealed by the Phase-Sensitive X-ray Diffraction (PSXD) Technique

W. Yashiro and T. Takahashi

Strain near an interface affects its electronic structure, but a full understanding of such strains is still lacking even in the case of SiO_2/Si, which has been applied to electronic devices since 1960s. We have developed a new technique, the phase-sensitive X-ray diffraction (PSXD) technique, which is a powerful way to characterize strain fields near crystal surfaces. By using this technique we have revealed that there is a small strain field extending over mesoscopic-range depth (up to several hundred of nm) under the SiO_2/Si interface and having a static fluctuation in the lateral direction [1]. This technique can also be applied to investigate

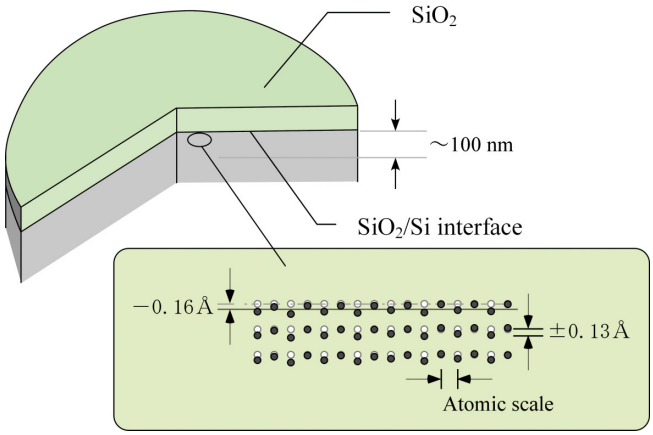

Fig. 1. An illustration of the strain field in a Si(001) wafer on which a thermal oxide layer was formed. The open circles represent the sites of atoms or unit cells in bulk crystal, and the solid circles represent the position of them in the strained layer near the interface. The arrangement of the experiment was set to be particularly sensitive to strain fields distributing mesoscopic-range depth. The phase shift of modulation profile can be simply interpreted into the sum of displacements of atomic planes under the interface projected onto the direction perpendicular to the 004 plane. Our experimental results showed that there is a total displacement of -0.16 Å in the direction perpendicular to the crystal surface. On the other hand the experimentally obtained visibility indicates that the total displacement has static fluctuation in the direction parallel to the interface. The visibility was interpreted into a static fluctuation of at least ± 0.13 Å in the lateral direction.

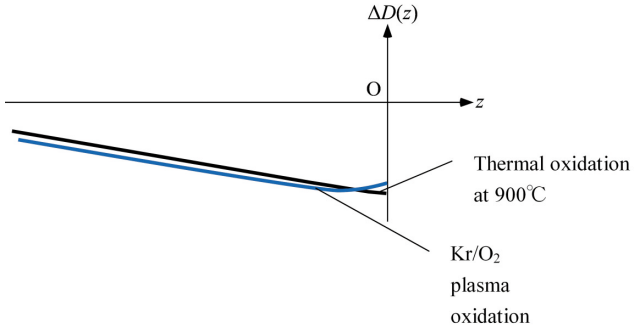

Fig. 2. A schematic view of the distribution of strain fields under the SiO_2/Si interfaces in the cases of Kr/O_2 plasma oxidation and thermal oxidation at 900℃, which was revealed by using the PSXD technique. It was shown that the distribution of strain field under the Kr/O_2 plasma oxide layer a few nanometer thick was different from that under the thermal oxide layer very near to the interface. Here $\Delta D(z)$ is the total displacement atomic planes under the SiO_2/Si interface and z is the depth, the origin of which is defined at the interface.

distribution of strain field under the interface.

The PSXD technique is an application of a phenomenon, modulation of the intensity of the crystal-truncation-rod (CTR) scattering under an excitation of a Bragg reflection [1-3], which is an interaction between a two-dimensionally diffracted wave (CTR scattering) and a three-dimensionally diffracted (Bragg reflection) wave. It was shown that the modulation profile can be characterized by two parameters: the phase shift, which represents the dip or peak position of the modulation profile, and the visibility. The phase shift can be simply interpreted into the sum of displacements of atomic planes under the interface, which is due to the strain field extending over mesoscopic-range depth, while the visibility gives information on static fluctuation of the total displacement in the lateral direction.

Figure 1 shows an illustration of strain field under a SiO_2/Si interface which was revealed by the PSXD technique [1]. The experimentally obtained phase shift was interpreted into a total displacement of -0.16 Å under the interface projected onto the direction perpendicular to the 004 plane. On the other hand the experimentally obtained visibility indicated that the total displacement has a static fluctuation of at least ± 0.13 Å in the direction parallel to the interface. Another example of the result of the PSXD technique is shown in Fig. 2, where the distributions of strain fields under the SiO_2/Si interfaces are illustrated in the cases of Kr/O_2 plasma oxidation and thermal oxidation at 900℃. These features revealed by the PSXD technique are expected to provide a new window to understand the oxidation mechanism of Si surface.

References

[1] W. Yashiro, K. Sumitani, T. Takahashi, Y. Yoda, and K. Miki, Surf. Sci. **550**, 93 (2004).
[2] T. Takahashi and S. Nakatani, Surf. Sci. **326**, 347 (1995).
[3] W. Yashiro, K. Sumitani, Y. Yoda, and T. Takahashi, Jpn. J. Appl. Phys. **42**, 6658 (2003), and references therein.

Authors

W. Yashiro[a], K. Sumitani, Y. Yoda[c], K. Miki[a,b], K. Takahashi[d], T. Hattori[d], and T. Takahashi

[a] Nanomaterials Laboratory (NML), National Research Institute for Materials Science (NIMS)
[b] Graduate School of Pure and Applied Sciences, University of Tsukuba
[c] Japan Synchrotoron Radiation Research Institute (JASRI)
[d] Department of Electrical and Electronic Engineering, Faculty of Engineering, Musashi Institute of Technology

New Type of Universality on Néel Temperatures of Quasi-Low-Dimensional Antiferromagnets

C. Yasuda, S. Todo, and H. Takayama

While the genuinely two-dimensional (2D) and one-dimensional (1D) antiferromagnetic Heisenberg (AFH) models cannot display long-range order except at zero temperature, weak inter-layer or inter-chain couplings, J', which always exist in real materials, lead to a phase transition at a finite Néel temperature T_N. So far, the J'-dependence of T_N was calculated by exactly treating effects of the strong interaction J in the 2D or 1D system, but by using mean-field-type approximations for effects of J'. The results are widely utilized for analyses of experimental measurements for quasi-low-dimensional (QLD) antiferromagnets, e.g., the quasi-2D (Q2D) high-T_c superconductor La_2CuO_4, the quasi-1D (Q1D) antiferromagnet Sr_2CuO_3, and so on.

Recently we have performed large-scale Monte Carlo (MC) simulations on anisotropic cubic lattices as a subject of the joint-use of the ISSP supercomputer system. Besides useful and quantitatively more accurate formulae for T_N, we obtained a new type of universal behavior of T_N for the QLD AFH models.[1] Our numerical work shows

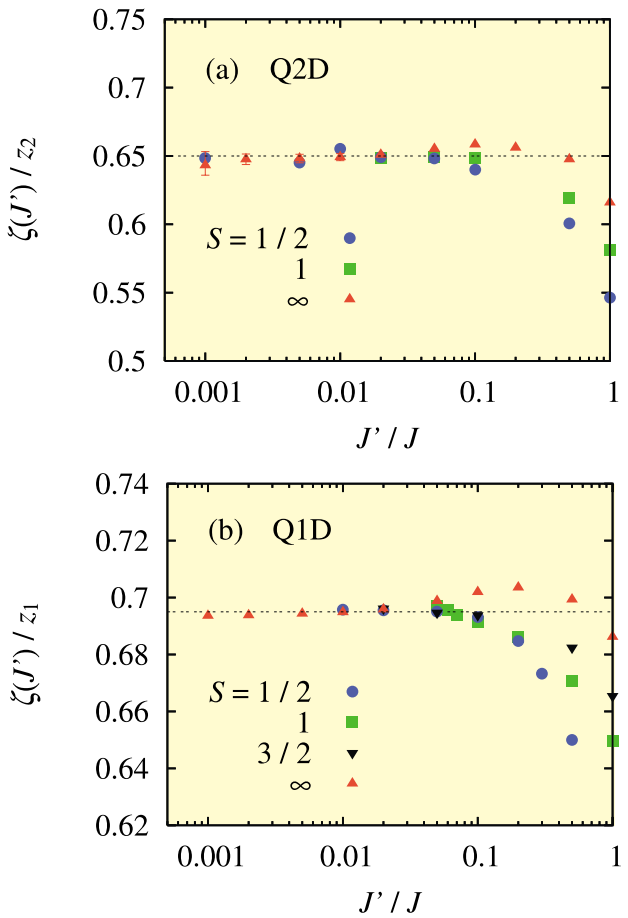

Fig. 1. Values of $\zeta(J')/z_d$ of the Q2D (a) and Q1D (b) AFH models. They are evaluated from T_N which are obtained from the finite-size scaling analysis on our numerical data for the QLD system and $\chi_s(T_N)$ which are obtained also from MC simulations interpolated near $T = T_N$. An exception here is χ_s of the classical 1D model, for which its known exact solution is used. Another comment is on the S=1 Q1D system, that simulations at lower temperature than the Haldane gap of the isolated chain are hardly carried out and so our analysis is limited in the range of $J'/J \geq 0.05$. The error bar of each point is smaller than the symbol size unless given explicitly.

that a renormalized coordination number defined by $\zeta(J') \equiv 1/J'\chi_s(T_N)$ becomes constant $\zeta(J') \approx \zeta_d = k_d z_d$ not depending on J' for $J' < J'_c \simeq 0.1J$ as shown in Fig. 1. Here, $\chi_s(T)$ is the staggered susceptibility of the 2D or 1D model at temperature T and z_d is the coordination number, $z_{2\,(1)} = 2$ (4) for the Q2D (Q1D) system. When $k_d = 1$, this relation reduces to the well-known RPA result: $z_d J'\chi_s(T_N) = 1$. Interestingly, the values of k_d are found to be common within our numerical accuracy for S=1/2, 1, 3/2 and ∞.

For the Q2D systems, $T_N(J') \propto -1 / \ln(J'/J)$ is expected at small J'/J for both quantum and classical systems from their common exponential forms of χ_s at $T \to 0$. Figure 1 (a) shows that the values of $\zeta(J')$ and so $k_2 = 0.65$ are universal, or independent of the spin size S. Using the analytical form of χ_s obtained in the renormalized classical regime of the non-linear σ model (NLσM), our universal relation is compatible with the one derived analytically for the S= 1/2 Q2D AFH model in the limit $J'/J \to 0$.[2] For the Q1D systems, due to the different forms of χ_s, we observe that $T_N(J') \propto \sqrt{J'/J}$ at small J'/J for $S = \infty$, while $T_N(J') \propto J'/J$ with logarithmic corrections for S=1/2. In spite of this difference, as shown in Fig. 1 (b), the values of $\zeta(J')$ are universal with k_1= 0.695 again for $J'/J \lesssim 0.1$. Moreover, the value of k_1 is quantitatively consistent with the result $k_1 \simeq 0.70$ of the modified RPA theory, in which the $1/z_1$ corrections to the inter-chain mean-field theory have been obtained by means of the bosonized Hamiltonian of the S=1/2 Q1D AFH model.[3]

The independence of ζ_d on the spin size S for the QLD systems suggests a universality of corrections to RPA for $J' \ll J$. Since in this temperature regime the physics of all these models should be well described by an anisotropic NLσM in the renormalized classical regime, we conjecture universal corrections to RPA also for the NLσM.

References

[1] C. Yasuda *et al.*, to be published in Phys. Rev. Lett. (cond-mat/0312392).
[2] V. Yu. Irkhin and A. A. Katanin, Phys. Rev. B **55**, 12318 (1997).
[3] V. Yu. Irkhin and A. A. Katanin, Phys. Rev. B **61**, 6757 (2000).

Authors

C. Yasuda[a], S. Todo[b], K. Hukushima[c], F. Alet[d], M. Keller[e], M. Troyer[e,f], and H. Takayama

[a] Department of Physics and Mathematics, Aoyama Gakuin University
[b] Department of Applied Physics, University of Tokyo
[c] Department of Basic Science, University of Tokyo
[d] Servie de Physique Théorique, CEA Saclay
[e] Theoretische Physik, ETH Zürich
[f] Computational Laboratory, ETH Zürich

Superconductivity in Water-Intercalated Tantalum Sulfides

M. Nohara and F. Sakai

Water, one of the most common molecule around human life, has not been recognized its major role in solid state physics until the discovery of watery superconductivity in the layered cobalt oxide Na_xCoO_2 [1]. The superconductivity at about 5 K emerges when the water molecules are intercalated between the CoO_2 and Na layers, namely, the CoO_2 layers are separated by a "bilayer" of water molecules. Remarkably, the superconductivity disappears when the CoO_2 layers are separated by a "monolayer" of water molecules, or the water molecules are absent between the layers.

In this joint research, we have discovered another family

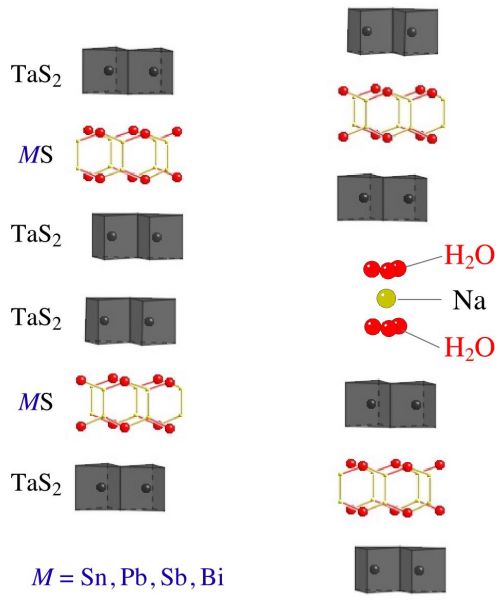

Fig. 1. Schematic view of the crystal structure of "parent" compound $(MS)_{1+\delta}(TaS_2)_2$ and "bilayer" hydrate $Na_x(H_2O)_y(MS)_{1+\delta}(TaS_2)_2$. The water molecules are intercalated between the TaS_2 and Na layers.

of water-intercalated superconductors in novel hydrate sulfides $Na_x(H_2O)_y(MS)_{1+\delta}(TaS_2)_2$ with M = Sn, Pb, Sb, and Bi. The parent compound $(MS)_{1+\delta}(TaS_2)_2$ consists of a pair of $(TaS_2)_2$ layers and a rock-salt layers of MS, as shown in Fig. 1. Na ions and water molecules are intercalated between the adjacent TaS_2 layers and anhydrate $Na_x(MS)_{1+\delta}(TaS_2)_2$ and "bilayer" hydrate $Na_x(H_2O)_y(MS)_{1+\delta}(TaS_2)_2$ are obtained. The chemical composition of these materials was successfully determined at *Materials Design and Characterization Laboratory, ISSP*, by using various facilities including an electron-probe microanalyser (EPMA). Figure 2 shows superconducting transition observed for the M = Sb series. The transition temperature T_c increases as the Na ions and water molecules are intercalated. Remarkably, the hydrate exhibits the highest T_c. Since the Na content is the same for both the hydrate $Na_x(H_2O)_y(SbS)_{1+\delta}(TaS_2)_2$ and anhydrate $Na_x(SbS)_{1+\delta}(TaS_2)_2$, this indicate that the water molecules are favorable to superconductivity in the sulfides as well as in the Co oxide. We naively expect that the T_c is reduced by random Coulomb potential created by Na ions on the conducting TaS_2 layers for the anhydrate, and the potential is effectively shielded by the water molecule indebted to its large polarization. The detail has been published in Ref. 2.

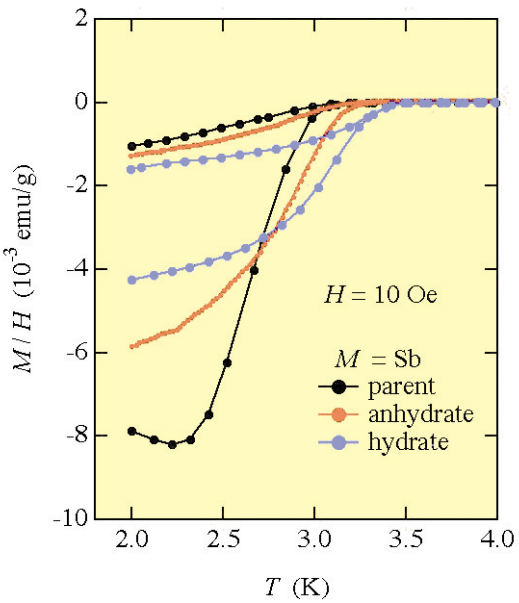

Fig. 2. Temperature dependence of magnetic susceptibility for parent $(SbS)_{1+\delta}(TaS_2)_2$, anhydrate $Na_x(SbS)_{1+\delta}(TaS_2)_2$, and hydrate $Na_x(H_2O)_y(MS)_{1+\delta}(TaS_2)_2$. Superconducting transition temperature is enhanced by water molecules.

References
[1] K. Takada *et. al*., Nature **422**, 53 (2003).
[2] N. Katayama, M. Nohara, F. Sakai, and H. Takagi, J. Phys. Soc. Jpn. **74**, 851 (2005).

Authors
N. Katayama[a], M. Nohara[a], H. Takagi[a], and F. Sakai
[a] Department of Advanced Materials Science, University of Tokyo

X-ray Study at Low Temperature and Under Pressure in $(TMTSF)_2FSO_3$

J. Yamaura and W. Kang

Bechgaard salt $(TMTSF)_2FSO_3$ is an interesting molecular conductor, indicating the complex pressure-temperature phase diagram as shown in Fig. 1 [1]. The symbols are defined as the phase boundary: metal-insulator (I), anomaly in resistivity (II, III, VI), metal-superconductor (IV), and metal-metal (V). The FSO_3^- anion having a finite electric dipole moment is presumably related to an additional degree of freedom. Here, we investigated the origin of the transitions by X-ray diffraction measurements at low temperature and under pressure.

A single-crystal superstructure analysis including the (1/2,1/2,1/2) reflections were performed below the metal-insulator transition (89K) at ambient pressure. The orientational ordering of the anions, the tetramerization and the charge disproportionation of TMTSF molecules with a symmetry breaking were determined. The net moment of the electric dipoles of anions is directed to the TMTSF column (a-axis), which suggests the existence of ferroelec-

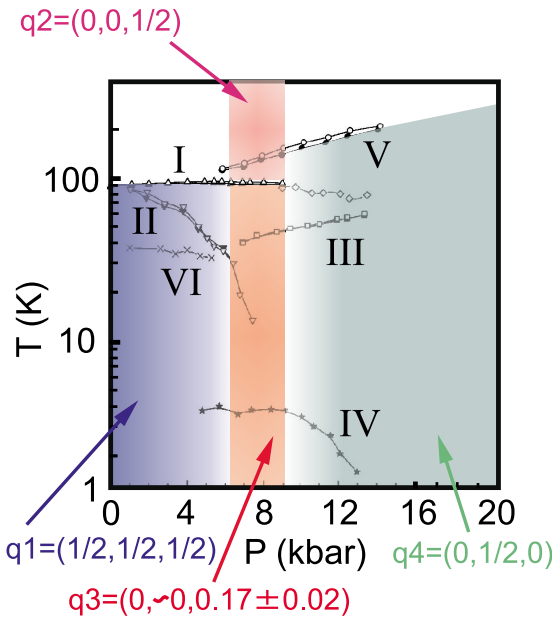

Fig. 1. Pressure-temperature phase diagram of $(TMTSF)_2FSO_3$. The symbols are defined as the phase boundary: metal-insulator (I), anomaly in resistivity (II, III, VI), metal-superconductor (IV), and metal-metal (V).

tricity. From the oscillation photograph using an imaging plate and a diamond anvil cell, we observed various types of satellite reflections: q_1=(1/2,1/2,1/2), q_2=(0,0,1/2), q_3=(0,≈0,0.17±0.02) and q_4=(0,1/2,0), as shown in Fig. 1. These are thought to originate from the orientational ordering of anions. In addition, a symmetry change from the triclinic *P*-1 to the monoclinic *P*m was observed accompanied with the q_4-superlattice through the transition V.

Reference

[1] Y. J. Jo, E. S. Choi, Haeyong Kang, W. Kang, I. S. Seo, and O. H. Chung, Phys. Rev. B **67,** 014516 (2003).

Authors

J. Yamaura, Y. J. Jo[a], Haeyong Kang[a], O. H. Chung[b], and W. Kang[a]
[a] Dept. of Physics, Ewha Womans University,
[b] Dept. of Physics, Sunchon University

ISSP Workshop

1. Recent progress and new frontiers of surface science using LEEM (low energy electron microscope) and PEEM (photoemission electron microscope)

April 26-27, 2004

T. Kinoshita and T. Koshikawa

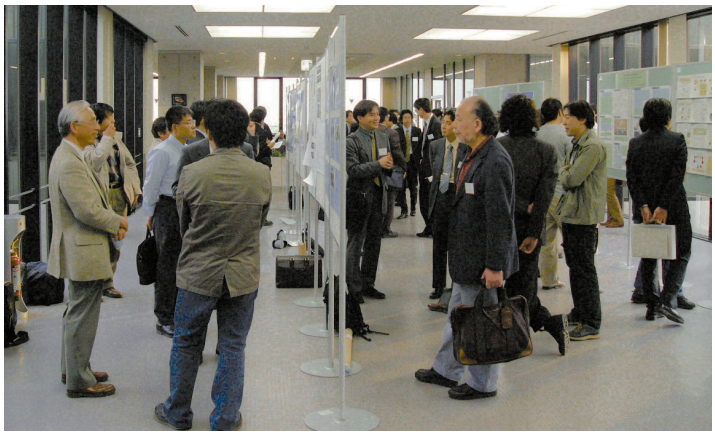

LEEM and PEEM are relatively new microscopic methods and attracted much attention because these give us a variety of experimental possibilities such as imaging, diffraction, micro-spectroscopy, dynamical observation and so on. The studies in this field become very active recently in Japan. This workshop was organized for the discussion and communication between the scientists who are using LEEM and/or PEEM. For such kind of microscopy techniques, the high brilliant light source in VUV and soft-X-ray regions is necessary, namely Super-SOR. The user's communities of the Super-SOR co-organized the workshop.

This workshop was a first full-scale meeting for LEEM/PEEM in Japan. Therefore some lectures concerning to LEEM and PEEM principles and recent activities were organized together with the oral- and the poster-sessions. It was confirmed that the LEEM/PEEM are very useful for the studies of the dynamical observation of thin-films and nanostructure growth, catalysis reaction, element-specific magnetic domain observation, and characterization of devices/ recording media etc. Further, some PEEM apparatus have been installed in the synchrotron radiation facilities, PF, HiSOR, and Spring-8. Some of them have been opened to the outside-users. The demands from users and information concerning to the apparatus were discussed.

At the end of the workshop, the present status of the Super-SOR project was introduced. The requests from the users to the beamlines were also discussed, for example, resolution, beam-size, polarization switching etc. Especially in the field of LEEM/PEEM, high-brilliance light source is most important facilities. Frontiers of the surface science will be surely developed by the combination of Super-SOR and high-performance LEEM/PEEM.

http://www.issp.u-tokyo.ac.jp/contents/seminar/short/tanki20040426.html
http://www.issp.u-tokyo.ac.jp/labs/sor/button/leempeem-all.pdf

2. Peculiar magnetic properties in itinerant-electron systems and their application to magnetic material

May 13-15, 2004

H. Yamada

Theoretical and experimental studies on itinerant-electron magnetism were carried out in 1970' and 1980' intensively. Those basic studies have made a strong contribution to the recent progress in magnetism for various kinds of intermetallic compounds. These developments in this field are also much indebted to a rapid improvement of experimental techniques under multiple extreme conditions of high magnetic field and high pressure, and to the improvement of sample preparation. Furthermore, it became possible to discuss theoretically the peculiar magnetic properties observed in 3d transition-metal compounds, by using calculated band-structures of electrons and by taking into account the effect of spin fluctuations. Under strong collaborations between theory and experiment, the basic study on magnetism in the itinerant-electron system has been developed intensively in Japan. On the other hand, it is not too much to say that the recent progress in the studies on applied science, not only of giant magnetostrictive, giant magnetocaloric materials but also of ferromagnetic shape memory, thermoelectric, and half-metal materials, is based on the basic researches of magnetism in the itinerant-electron system. In order to make a strong collaboration between these basic and applied sciences further, the present meeting was held. Including two foreign researchers, 37 papers on current topics in basic and applied magnetism of the itinerant-electron system were presented. About 100 participants, including graduated students, have attended to this meeting and a lot of exciting discussions have been done.

http://www.issp.u-tokyo.ac.jp/contents/seminar/short/tanki20040513.html

3. Physical properties and energy landscapes of extremely non-equilibrium systems

August 9-10, 2004

O. Yamamuro, H. Takayama, and M. Shibayama

Recently, the non-equilibrium systems extremely apart from their equilibrium states attract attentions of many scientists. Various amorphous materials, polymer and supramolecular systems, and biomaterials such as proteins are included in this category. Their potential energy and free energy surfaces in configurational space, so-called "energy landscape", have many basins corresponding to their many metastable states. It is considered that the shape of the basins and the transformation among the basins dominate physical properties, relaxation processes and functions of the systems. The present workshop consisted of 21 oral and 21 poster presentations for the experimental and theoretical studies on glass transitions, amorphous ices, spin glasses, polymer crystallization, gels, proteins, etc. About 80 participants actively discussed the new theoretical approach for the landscape, the explanation of various physical properties using the landscape, and the future development for the landscape science.

http://yamamuro.issp.u-tokyo.ac.jp/workshop1.html

4. Frontier and new field of science opened by VUV/SX third generation high-brilliance synchrotron radiation

December 9-11, 2004

H. Daimon, A. Kakizaki, J. Yoshinobu, and T. Kinoshita

The project for constructing a new third-generation synchrotron radiation facility dedicated to sciences in VUV and Soft X-ray (SX) region has been eagerly awaited by many people for a long time. Although there is no third-generation VUV/SX ring in Japan, many researchers are conducting unique and cutting-edge science in this field using second-generation rings or those in foreign countries.

One aim of this symposium is to survey frontier condensed-matter and nanosciences conducted by advanced Japanese researchers. A lot of presentations and active discussions occurred throughout the three days. It was recognized that many fruitful advanced activities are being done in this field by young scientists and new fields will be created by the new third-generation synchrotron radiation facility. There are many users who desire to use the ring.

Another aim of this symposium is to increase the number of users of the new third-generation synchrotron radiation facility. The Kashiwa campus, which is the most probable location of the ring, is close to other scientific and technological institutes, such as Tokatsu Techno Plaza, National Cancer Center, National Research Institute of Police Science, and Faculty of Horticulture of Chiba University. Only a one-day trip would be required to use the facility for the people in Tokyo bay area, where many potential users exist in industry of nano-analysis, nano-fabrication, and medical- or bio-science. We asked some researchers and technical experts of these industries to present their request during the symposium. A ring which fulfills these requirements is hoped for.

http://www.issp.u-tokyo.ac.jp/contents/seminar/short/tanki20041209.html

5. French-Japanese meeting on high magnetic field

December 6, 2004

S. Takeyama and M. Takigawa

Static high magnetic field provides valuable opportunities to discover novel phenomena in condensed matter science. Quantum phase transitions induced by magnetic field in spin systems, organic conductors and semiconductors, and novel magneto optical effects are good examples. This workshop was organized to stimulate collaboration between Japanese scientists interested in research using static high magnetic field and the Grenoble High Magnetic Field Laboratory (GHMFL), which provide excellent experimental environment at high field up to 33 tesla and at low temperature. In the first half of the meeting, French participants including Dr. G. Martinez, the director of GHMFL, explained the operation of the facility, technical aspects of magnet design, capabilities for various condensed matter experiments such as NMR, EPR, optical measurements and transport measurements. In the second half, the Japanese participants presented several experimental proposals as well as distinct features of the high field facility in Tohoku University. We hope that fruitful collaboration will come out as a results of such workshop.

http://www.issp.u-tokyo.ac.jp/labs/extreme/himag-forum/page013.html

6. The structure of the Si(111)-$\sqrt{3}\times\sqrt{3}$ -Ag surface and its phase transition

December 14- 15, 2004

T. Takahashi

The structure of the Si(111)-$\sqrt{3}\times\sqrt{3}$ -Ag surface has been attracting interests over thirty years since the first observation of the surface by low energy electron diffraction. After a long controversy the structure at room temperature was determined by x-ray diffraction, but recent studies by first-principles calculations and STM at low temperature suggest that a slightly different structure with a rotation is more stable at low temperatures. In this workshop the structure of the surface at both high and low temperature phases as well as the phase transition is intensively discussed.

http://www.issp.u-tokyo.ac.jp/contents/seminar/short/tanki20041214.html

7. To new science with SANS, QENS, and NSE

January 26-27, 2005

M. Shibayama

The Neutron Science Laboratory, (NSL-ISSP) has upgraded three major instruments covering the fields of soft matter physics, glasses, mixtures, and biological systems. The instruments were SANS-U (**S**mall **A**ngle **N**eutron **S**cattering Instrument, **U**niversity of Tokyo), iNSE (New **i**SSP **N**eutron **S**pin **E**cho Spectrometer), and AGNES (**A**n**g**le Focusing Cold **Ne**utron **S**pectrometer). The purposes of the workshop were to demonstrate the performance of these instruments and to discuss the recent topics in these fields. The workshop consisted of instrumentation and cross-disciplinary sections, namely, introduction of the upgraded instruments, biology and high performance polymer, new aspects of soft matter physics, physics of mixtures, and slow dynamics of glasses, etc. Active discussions with 65 participants related to 25 oral presentations and 23 posters were quite meaningful to predict the directions of new sciences. The presentation record of the workshop was issued as an NSL News Letter 2005-1 in June, 2005.

http://shibayama.issp.u-tokyo.ac.jp/ISSPWS/ISSPWS0501.html)

8. Electronic transport in magnetic systems

February 14-15, 2005

Y. Iye, T. Ono, Y. Otani, T. Kato, and S. Katsumoto

Study of electronic transport in magnetic systems has a long history in magnetic materials such as transition and rare earth metals and alloys. In recent years, the scope has been immensely widened by the advent of diluted magnetic semiconductors and transition metal oxides. Research in this field is entering a new phase by the ability of fabricating artificial structures by the technical developments of thin film growth and microfabrication. On the theoretical side, there is growing interest in novel quantum transport phenomena associated with geometrical phase. Recent topics include, electrons scattering at the domain boundary in ferromagnetic metals, control of domain wall motion by spin polarized current, observation of domain wall dynamics, spin injection in magnetic and non-magnetic semiconductor hybrid structures, and spin Hall effect. In this workshop, active researchers in this field presented their latest results and exchanged the ideas.

http://iye.issp.u-tokyo.ac.jp/Workshop/ISSP-workshop.htm

9. High pressure material seminar21:Frontier of Megabar Science

March 4, 2005

Y. Uwatoko

A high-pressure technology has contributed to advancements of researches in solid state physics. The number of the subjects increases when a new high-pressure technology appeared, and a lot of new physical properties have been found. New physical phenomenon and function seems to be still waiting to be discovered by us under the high pressure. This seminar was programmed with 3 sessions of; technology for very high-pressure generation, search for new physical properties under pressure, high-pressure synthesis of new functional materials. Organizer proceeded to a discussion in above subjects in one megabar (1 million atmospheric pressure) class pressure region.

http://www.issp.u-tokyo.ac.jp/contents/seminar/short/highpressure21-20050304.html